Thermally Stable and Highly Efficient *N,N,N*-Cobalt Olefin Polymerization Catalysts Affixed with *N*-2,4-Bis(Dibenzosuberyl)-6-Fluorophenyl Groups

Muhammad Zada [1,2], Desalegn Demise Sage [1], Qiuyue Zhang [1], Yanping Ma [1], Gregory A. Solan [1,3,*], Yang Sun [1] and Wen-Hua Sun [1,*]

1   Key Laboratory of Engineering Plastics, Beijing National Laboratory for Molecular Sciences, Institute of Chemistry, Chinese Academy of Sciences, Beijing 100190, China
2   Department of Chemistry, Government Postgraduate College Khar, Bajaur 18650, Pakistan
3   Department of Chemistry, University of Leicester, University Road, Leicester LE1 7RH, UK
*   Correspondence: gas8@leicester.ac.uk (G.A.S.); whsun@iccas.ac.cn (W.-H.S.); Tel.: +44(0)-116-2522096 (G.A.S.); +86-10-62557955 (W.-H.S.)

Abstract: The cobalt(II) chloride *N,N,N*-pincer complexes, [2-{(2,4-($C_{15}H_{13}$)$_2$-6-FC_6H$_2$)N=CMe}-6-(ArN=CMe)C_5H$_3$N]CoCl$_2$ (Ar = 2,6-Me$_2$$C_6H_3$) (**Co1**), 2,6-Et$_2$$C_6H_3$ (**Co2**), 2,6-*i*-Pr$_2$$C_6H_3$ (**Co3**), 2,4,6-Me$_3$$C_6H_2$ (**Co4**), 2,6-Et$_2$-4-MeC_6H$_2$ (**Co5**), and [2,6-{(2,4-($C_{15}H_{13}$)$_2$-6-FC_6H$_2$)N=CMe}$_2$$C_5H_3$N]CoCl$_2$ (**Co6**), each containing at least one *N*-2,4-bis(dibenzosuberyl)-6-fluorophenyl group, were synthesized in good yield from their corresponding unsymmetrical (**L1**–**L5**) and symmetrical bis(imino)pyridines (**L6**). The molecular structures of **Co1** and **Co2** spotlighted their distorted square pyramidal geometries (τ_5 value range: 0.23–0.29) and variations in steric hindrance offered by the dissimilar *N*-aryl groups. On activation with either MAO or MMAO, **Co1**–**Co6** all displayed high activities for ethylene polymerization, with levels falling in the order: **Co1** > **Co4** > **Co5** > **Co2** > **Co3** > **Co6**. Indeed, the least sterically hindered 2,6-dimethyl **Co1** in combination with MAO exhibited a very high activity of 1.15×10^7 g PE mol^{-1} (Co) h^{-1} at the operating temperature of 70 °C, which dropped by only 15% at 80 °C and 43% at 90 °C. Vinyl-terminated polyethylenes of high linearity and narrow dispersity were generated by all catalysts, with the most sterically hindered, **Co3** and **Co6**, producing the highest molecular weight polymers [M_w range: 30.26–33.90 kg mol^{-1} (**Co3**) and 42.90–43.92 kg mol^{-1} (**Co6**)]. In comparison with structurally related cobalt catalysts, it was evident that the presence of the *N*-2,4-bis(dibenzosuberyl)-6-fluorophenyl groups had a limited effect on catalytic activity but a marked effect on thermal stability.

Keywords: cobalt; ethylene polymerization; dibenzosuberyl; *ortho*-fluoride; thermal stability; linear polyethylene; high activity

1. Introduction

The deployment of late transition metal (e.g., Fe, Co, Ni, Pd) complexes as catalysts in ethylene polymerization has been extensively investigated since the groundbreaking discoveries in the mid-to-late 1990′s [1–4]. Much of the interest in the area stems from their ease of preparation and their ability to generate various types of industrially important polyethylenes, ranging from highly linear to highly branched with differing levels of end-group unsaturation [3–6].

Regarding iron and cobalt catalysts, most incorporate the tridentate 2,6-bis(arylimino) pyridine ligand frame (**A**, Figure 1). Indeed, for this class of catalyst, numerous studies have been dedicated to exploring the relationships between structure and productivity, as well as the properties of the resulting polymers [1,2]. As a consequence, factors such as the choice of metal center and the substitution pattern displayed by the *N,N,N*-ligand have been shown to be of crucial importance. Furthermore, such variations to the chelating ligand structure

can also impact the thermal stability of the catalyst, with poor thermal stability being a characteristic that has, in part, limited their industrial application [1,2,6–8]. In most cases, these structural modifications have been concerned with the *N*-aryl groups and, in particular, the influence of substituents with differing steric and electronic properties [1,2,5,8–22]. As a more recent modification, the fusion of carbocyclic rings to the central pyridine in **A** has seen improvements in both catalytic performance and thermal stability [23–35].
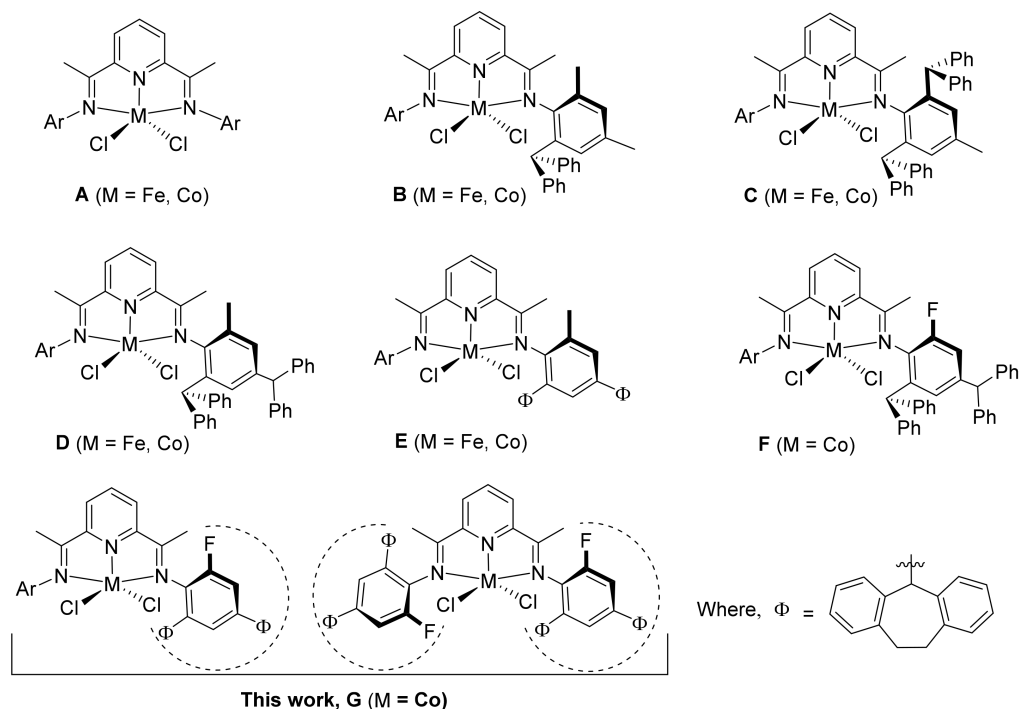

Figure 1. Structural modifications to the ligand framework in 2,6-bis(arylimino)pyridine-iron(II) and -cobalt(II) chloride complexes, **A**–**F**, including the target of this work, **G**.

As an on-going theme in our research, we have been interested in developing families of unsymmetrical bis(imino)pyridine–iron and –cobalt complexes that contain one fixed *N*-aryl group and the other variable. For example, precatalysts of type **B** (Figure 1) incorporate a *N*-2-benzhydryl-4,6-dimethylphenyl group as the fixed aryl group, while the other aryl group offers a means to fine-tune performance through steric and electronic variation. Indeed, iron and cobalt examples of **B** exhibit very good catalytic activity [36], while **C** (Figure 1), bearing two sterically hindered *ortho*-benzhydryl groups along with an electron-donating *para*-methyl group, not only display high catalytic activity but also enhanced thermal stability (**C**, Figure 1) [37–42]. Moreover, analogues of **C** with the *para*-methyl group replaced by electron-withdrawing substituents have seen further improvements, particularly for iron [39–47]. Incorporation of fluoride into the benzhydryl periphery has also led to catalysts displaying high activity and good thermal stability [43,44]. Elsewhere, the positioning of benzhydryl groups within the *N*-aryl ring has been the subject of a number of reports. For instance, cobalt-containing $\mathbf{D_{Co}}$ (Figure 1), affixed with a *N*-2,4-dibenzhydryl-6-methylphenyl group, exhibited exceptional catalytic activity (up to 18.1×10^6 g of PE mol^{-1} (Co) h^{-1}), while the thermal stability was somewhat reduced [48,49].

As a development of our work using benzhydryl as a substituent on the *N*-aryl ring, we have also been interested in employing dibenzosuberyl groups, in which the two phenyl groups in benzhydryl have been tethered by an ethyl linker [50–53]. For example, $\mathbf{E_{Co}}$ (Figure 1), the dibenzosuberyl equivalent of $\mathbf{D_{Co}}$, displayed comparatively higher thermal stability, while the polyethylene was of similarly high molecular weight [52,53]. As a more recent finding, the introduction of fluoride in conjunction with two benzhydryl groups on the *N*-aryl ring has seen the disclosure of cobalt-containing $\mathbf{F_{Co}}$ (Figure 1). Indeed, $\mathbf{F_{Co}}$

exhibited very high catalytic activity and superior thermal stability [54]. Similarly, the bis(4,4'-difluorobenzhydryl) counterpart of **F** showed promising performance in terms of catalytic productivity and thermostability [55,56].

In order to further refine our understanding of the factors that influence catalytic performance and temperature resilience in this type of polymerization catalyst, we targeted in this work a series of bis(imino)pyridine-cobalt precatalysts appended with *N*-2,4-bis(dibenzosuberyl)-6-fluorophenyl groups (**G**, Figure 1). We anticipated that the electronic effect of the 6-fluoride in close proximity to the central metal and the steric effect imposed by the dibenzosuberyl groups, along with the anticipated acidity of its methine protons, might have some impact on catalytic performance and particularly on thermal stability. With this in mind, we disclose five distinct examples of unsymmetrical cobalt precatalysts differing in the steric and electronic properties of the second *N*-aryl group and one symmetrical example bearing two *N*-2,4-bis(dibenzosuberyl)-6-fluorophenyl groups. These new complexes were subjected to a comprehensive polymerization evaluation that probed the type and amount of co-catalyst, reaction temperature, run time, and ethylene pressure. The results of this study are then compared to previously reported cobalt examples of **B**–**F** (Figure 1). In addition, the preparative details for the six novel 2,6-bis(imino)pyridines and their cobalt precatalysts are reported in detail.

2. Results and Discussion

The unsymmetrical 2,6-bis(arylimino)pyridines, 2-{(2,4-$(C_{15}H_{13})_2$-6-FC_6H_2)N=CMe}-6-(ArN=CMe)C_5H_3N (Ar = 2,6-$Me_2C_6H_3$) (**L1**), 2,6-$Et_2C_6H_3$ (**L2**), 2,6-*i*-$Pr_2C_6H_3$ (**L3**), 2,4,6-$Me_3C_6H_2$ (**L4**), and 2,6-Et_2-4-MeC_6H_2 (**L5**), were obtained in two steps in satisfactory overall yield (Scheme 1). Firstly, the condensation of 2,6-diacetylpyridine with one molar equivalent of *N*-2,4-bis(dibenzosuberyl)-6-fluoroaniline afforded the imine-ketone 2-{(2,4-$(C_{15}H_{13})_2$-6-FC_6H_2)N=CMe}-6-(O=CMe)C_5H_3N as the main product, along with some 2,6-{(2,4-$(C_{15}H_{13})_2$-6-FC_6H_2)N=CMe}$_2C_5H_3$N (**L6**) as the by-product. Treatment of the imine-ketone intermediate with the corresponding aniline, 2,6-R^1_2-4-$R^2C_6H_2NH_2$, under acid catalyzed conditions, gave **L1**–**L5**. The *N*-2,4-bis(dibenzosuberyl)-6-fluoroaniline was not commercially available and was prepared using a reported procedure [57–59].

Further reaction of **L1**–**L6** with anhydrous cobalt(II) chloride in a mixture of ethanol and dichloromethane generated [2-{(2,4-$(C_{15}H_{13})_2$-6-FC_6H_2)N=CMe}-6-(ArN=CMe)C_5H_3N]$CoCl_2$ (Ar = 2,6-$Me_2C_6H_3$) (**Co1**, 2,6-$Et_2C_6H_3$ (**Co2**), 2,6-*i*-$Pr_2C_6H_3$ (**Co3**), 2,4,6-$Me_3C_6H_2$ (**Co4**), 2,6-Et_2-4-MeC_6H_2 (**Co5**) and [2,6-{(2,4-$(C_{15}H_{13})_2$-6-FC_6H_2)N=CMe}$_2C_5H_3$N]$CoCl_2$ (**Co6**) in good yields (Scheme 1). All of the organic compounds were characterized by IR, ^{1}H, ^{13}C, and ^{19}F NMR spectroscopy and elemental analysis, while **Co1**–**Co6** were analyzed by elemental analysis, ^{19}F NMR, and IR spectroscopy, and **Co1** and **Co2** were analyzed by single crystal X-ray diffraction.

Single crystals of **Co1** and **Co2** employed for the X-ray studies were grown by slow diffusion of *n*-heptane into a dichloromethane solution of the corresponding complex. Perspective views of both are shown in Figures 2 and 3, while selected bond lengths and angles are provided in Table 1. Crystallographic parameters are given in the supporting information (Table S1 from Supplementary Materials). The structures of **Co1** and **Co2** were similar and will be described as a pair. Each comprised a single cobalt center bound by a *N,N,N*-chelating bis(arylimino)pyridine and two chloride ligands to complete a geometry that can be best described as distorted square pyramidal. More accurately, this distortion can be quantified using the geometric tau value (τ_5). This parameter can be defined from the equation $\tau_5 = (\beta-\alpha)/60$, where β is the largest angle and α is the second largest angle in the coordination sphere. A tau value of zero is indicative of a perfect square pyramid and a value of one for a perfect trigonal bipyramid [49–57,60–64]. For **Co1** and **Co2**, the τ_5 values were 0.23 and 0.29, respectively, reflecting some degree of distortion from a perfect square pyramid. In each structure, the three nitrogen atoms N1, N2, and N3, along with Cl1, formed the basal plane, while Cl2 occupied the apical site and the cobalt center itself sat above the basal plane, by approximately 0.147 Å and 0.137 Å, respectively. With regard to the cobalt-

nitrogen bond lengths, the central Co(1)–N(1) distance [2.035(2) Å **Co1**, 2.0512(12) Å **Co2**] was noticeably shorter than Co(1)–N(2) [2.238(2) Å **Co1**, 2.1810(12) Å **Co2**] and Co(1)–N(3) [2.260(2) Å **Co1**, 2.1784(11) Å **Co2**], indicating more effective coordination of the $N_{pyridine}$ with the cobalt atom. Similar findings have been reported in the literature [45,46,48–56]. For **Co1**, the exterior Co-N_{imine} bond lengths also showed some minor variation, with Co1-N3 slightly longer than Co1-N2, although this was not reproduced in **Co2**. The N(2)–C(8) [1.281(3)–1.2819(19) Å] and N(3)–C(2) [1.271(3)–1.2851(18) Å] bond lengths in both complexes were typical of C=N double bonds. In addition, the *N*-aryl planes were inclined towards the perpendicular with respect to the *N,N,N*-chelating plane, with some modest variation in the dihedral angles (76.3°, 78.3° **Co1**; 77.7°, 83.3° **Co2**). Similar inclinations have been observed in other unsymmetrical bis(arylimino)pyridine complexes [36–46,50–56]. As a variation between the two structures, the *ortho*-dibenzosuberyl group in **Co1** was positioned on the same side as apical Cl2, while in **Co2**, the *ortho*-fluoride adopted this position. Within each *ortho-/para*-substituted dibenzosuberyl group, the central seven-membered ring was puckered on account of the three sp³-hybridized carbon atoms. There were no intermolecular contacts of note.

L	L1	L2	L3	L4	L5
Co	Co1	Co2	Co3	Co4	Co5
R¹	Me	Et	iPr	Me	Et
R²	H	H	H	Me	Me
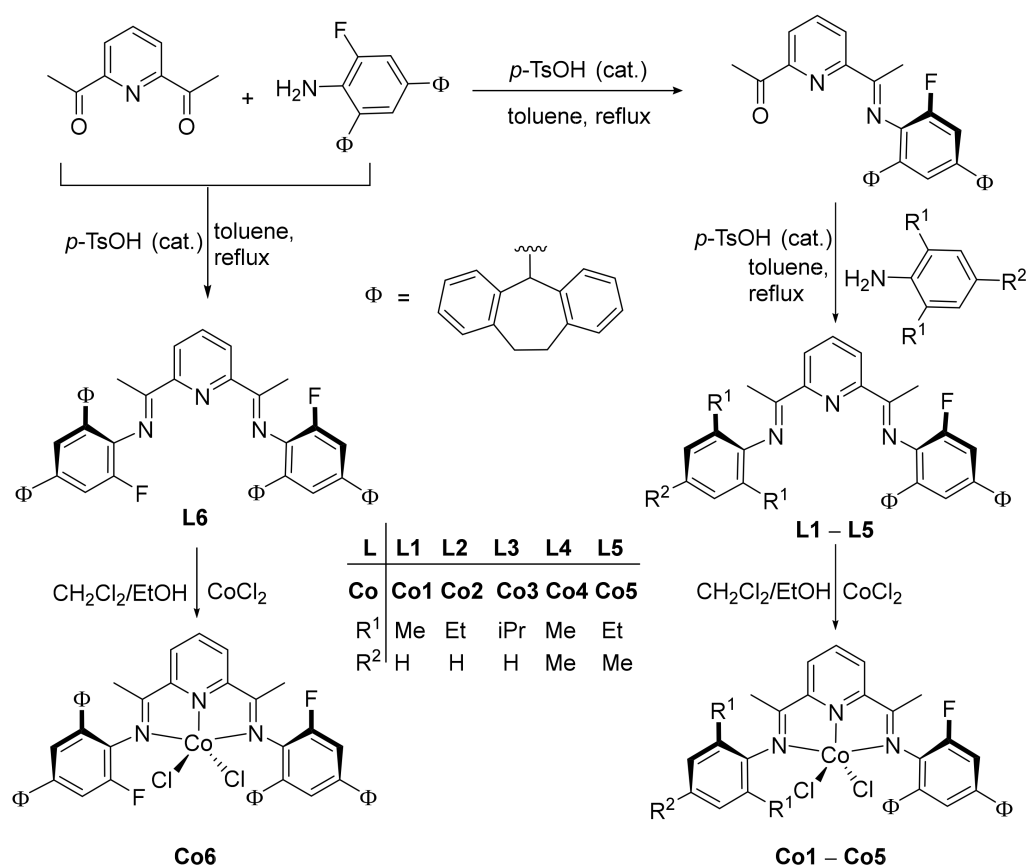
Scheme 1. Synthetic route to the bis(arylimino)pyridine derivatives (**L1–L6**) and their cobalt(II) chloride complexes (**Co1–Co6**).
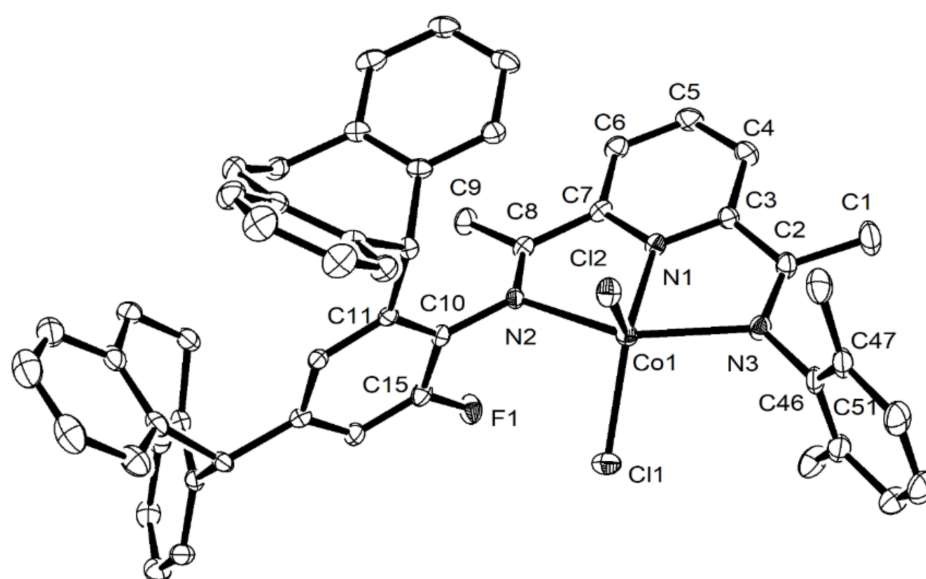
Figure 2. ORTEP representation of **Co1** with the thermal ellipsoids set at 30% probability level. All hydrogen atoms have been omitted for clarity.
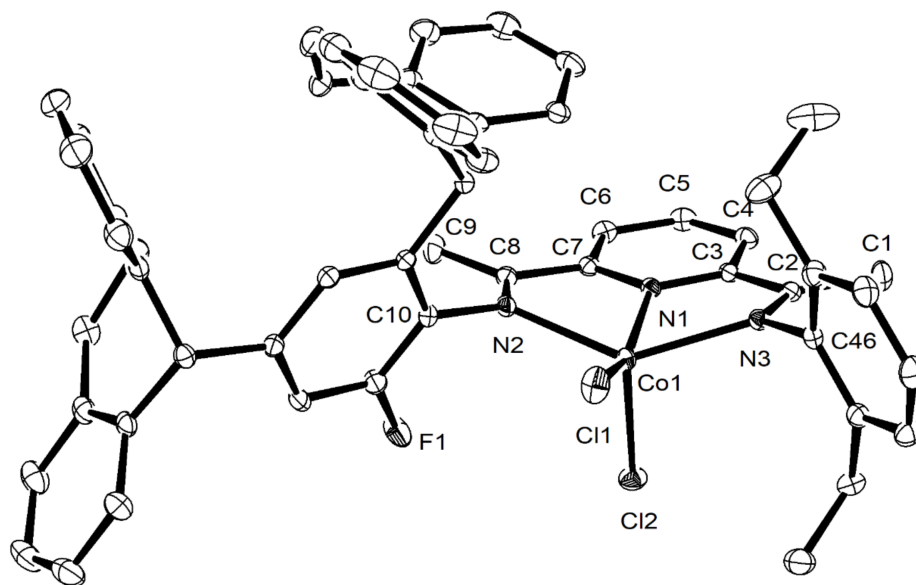
Figure 3. ORTEP representation of **Co2** with the thermal ellipsoids set at the 30% probability level. All hydrogen atoms have been omitted for clarity.

^{19}F NMR spectroscopy was performed on **L1**–**L6** and **Co1**–**Co6** in order to probe the effect of the fluorine environment and metal complexation on chemical shift. As expected, the spectra of the free ligands showed single peaks for the *ortho*-fluoride with chemical shifts of approximately δ −128.7 ppm (Figure S1 from Supplementary Materials), which compared to a range of between δ −146.9 and −129.3 ppm for **Co1**–**Co5** (see Figure 4 for representative spectra). Evidently, complexation with the paramagnetic Co(II) ion resulted in an upfield shift and a broadening of the fluorine resonances. Interestingly, the spectrum of symmetrical **Co6** showed major and minor peaks at δ −146.9 and −145.8 ppm, respectively (see Figure S2 from Supplementary Materials), which suggested the existence of two isomers in solution [55,56].

Table 1. Selected bond lengths (Å) and angles (°) for **Co1** and **Co2**.

	Co1	Co2
Bond Lengths (Å)		
Co(1)–N(1)	2.035 (2)	2.0512 (12)
Co(1)–N(2)	2.238 (2)	2.1810 (12)
Co(1)–N(3)	2.260 (2)	2.1784 (11)
Co(1)–Cl(1)	2.2370 (8)	2.2424 (4)
Co(1)–Cl(2)	2.2673 (8)	2.2960 (4)
N(2)–C(10)	1.437 (3)	1.4292 (18)
N(3)–C(46)	1.449 (3)	1.488 (2)
N(2)–C(8)	1.281 (3)	1.2819 (19)
N(3)–C(2)	1.271 (3)	1.2851 (18)
C(15)–F(1)	1.350 (3)	1.3591 (17)
Bond Angles (°)		
N(1)–Co(1)–N(2)	74.87 (8)	73.56 (4)
N(1)–Co(1)–N(3)	74.78 (8)	73.97 (4)
N(2)–Co(1)–N(3)	149.16 (8)	138.63 (4)
N(1)–Co(1)–Cl(1)	135.22 (6)	156.00 (4)
N(2)–Co(1)–Cl(1)	95.29 (6)	99.83 (3)
N(3)–Co(1)–Cl(1)	102.35 (6)	99.46 (3)
N(2)–Co(1)–Cl(2)	101.27 (6)	101.57 (3)
N(3)–Co(1)–Cl(2)	94.49 (6)	103.81 (3)
Cl(1)–Co(1)–Cl(2)	113.91 (3)	113.233 (18)
N(1)–Co(1)–Cl(2)	110.86 (6)	90.76 (3)
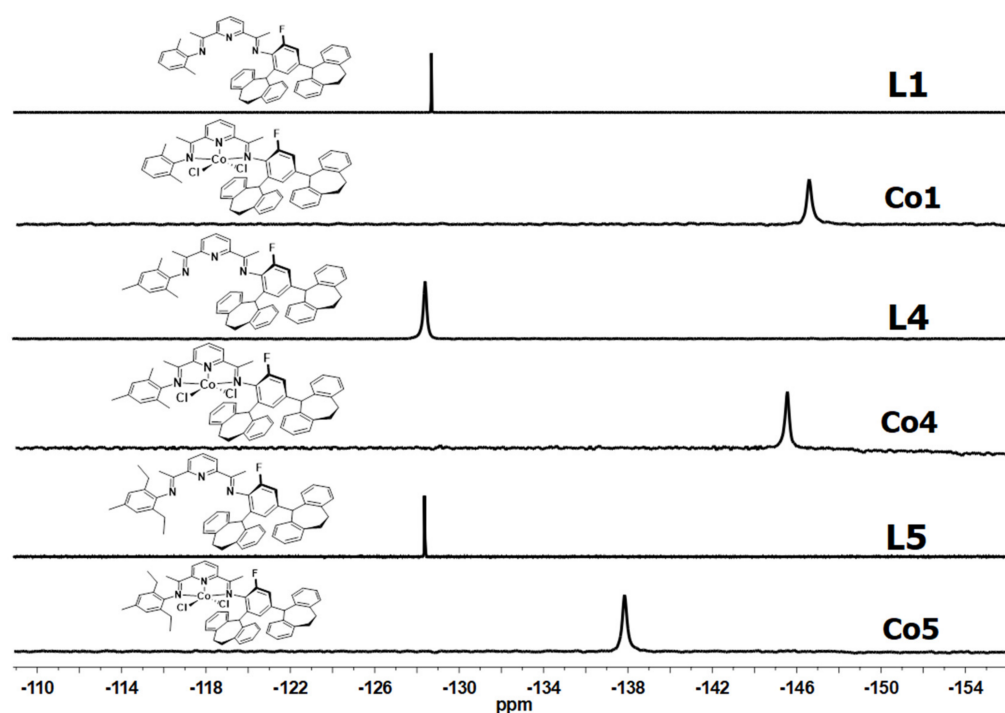
Figure 4. ^{19}F NMR spectra of **L1**, **L4**, and **L5**, along with those for their corresponding complexes **Co1**, **Co4**, and **Co5**; recorded in CDCl$_3$ at ambient temperature.

In the FT-IR spectra of **Co1**–**Co6**, the stretching vibrations for the C=N$_{imine}$ bonds appeared in the range of 1623–1632 cm^{-1}, which compared to 1641–1651 cm^{-1} for the free bis(imino)pyridines, **L1**–**L6**. This reduction in wavenumber was in accordance with the effective coordination of the imine nitrogen donor atoms to the metal center [36–39,48–57]. The elemental analyses of **Co1**–**Co6** were consistent with the proposed LCoCl$_2$ composition.

3. Ethylene Polymerization Studies

Previous work in the area indicated that aluminoxanes, such as MAO (methylaluminoxane) or MMAO (modified methylaluminoxane), are effective co-catalysts for generating the active bis(imino)pyridine-cobalt catalyst [13,14,36–42,48–57]. Accordingly, both MAO and MMAO were used during the catalytic evaluation of **Co1–Co6**, and their catalytic performance was compared. To identify an effective set of reaction conditions for the polymerizations, **Co1** was initially selected and parameters such as temperature, Al:Co molar ratio, run time, and ethylene pressure were systematically investigated with the ethylene pressure kept at 10 atm. All runs were performed in toluene as the solvent.

3.1. Optimization of Polymerization Conditions Using **Co1**/MAO

With **Co1**/MAO initially employed as the test catalyst system, the influence of run temperature was first investigated with the Al:Co molar ratio fixed at 2000:1 and the run time set at 30 min (runs 1–7, Table 2).

Table 2. Optimization of the polymerization conditions using **Co1**/MAO [a].

Run	T (°C)	t (min)	Al:Co	PE (g)	Activity [b]	M_w [c]	M_w/M_n [c]	T_m (°C) [d]
1	30	30	2000	1.82	2.43	16.80	2.43	130.4
2	40	30	2000	2.14	2.85	14.72	2.67	129.5
3	50	30	2000	2.83	3.77	11.15	2.63	128.9
4	60	30	2000	4.54	6.05	9.26	2.63	128.5
5	70	30	2000	8.61	11.48	7.40	2.42	127.7
6	80	30	2000	7.36	9.81	6.74	2.37	127.1
7	90	30	2000	4.92	6.56	5.44	2.27	126.1
8	70	30	1500	6.85	9.13	7.52	2.47	127.6
9	70	30	1750	8.02	10.70	7.75	2.37	128.2
10	70	30	2250	7.43	9.91	7.27	2.41	127.8
11	70	30	2500	6.37	8.49	7.07	2.29	127.8
12	70	30	3000	5.60	7.47	6.33	2.16	128.4
13	70	05	2000	2.57	20.56	6.73	2.27	127.3
14	70	15	2000	4.61	12.29	7.22	2.27	128.0
15	70	45	2000	9.02	8.02	7.53	2.46	127.6
16	70	60	2000	10.51	7.01	8.23	2.34	127.6
17 [e]	70	30	2000	3.87	5.16	6.27	2.55	127.2
18 [f]	70	30	2000	0.71	0.95	2.92	2.40	123.2

[a] General conditions: 1.5 μmol of **Co1**, 100 mL toluene, 10 atm C_2H_4, [b] 10^6 g of PE mol^{-1} (Co) h^{-1}, [c] M_w: kg mol^{-1}, determined by GPC, [d] determined by DSC, [e] 5 atm of C_2H_4, [f] 1 atm of C_2H_4.

When the temperature was increased from 30 to 70 °C, the catalytic activity steadily increased, reaching a peak level of 11.48×10^6 g of PE mol^{-1} of Co h^{-1} at the higher temperature (run 5, Table 2). Above 70 °C, some loss in activity was observed, with levels decreasing to 9.81×10^6 g of PE mol^{-1} of Co h^{-1} at 80 °C and then to 6.56×10^6 g of PE mol^{-1} of Co h^{-1} at 90 °C. Clearly, the active species generated using **Co1**/MAO displayed good thermal stability with only a 15% reduction in performance at 80 °C. It would seem probable that this latter dip in effectiveness was due to partial deactivation of the active species and/or lower solubility of the ethylene monomer at elevated temperature [36–46,49,52–57]. In contrast, the molecular weight of the polyethylene displayed a gradual decrease when the temperature increased from 30 to 90 °C, with M_w values dropping from 16.80 to 5.44 kg mol^{-1} (Figure 5). This reduction in molecular weight was ascribed to increased rates of chain transfer reactions as compared to chain propagation at higher run temperatures [38–46,49,52–55].
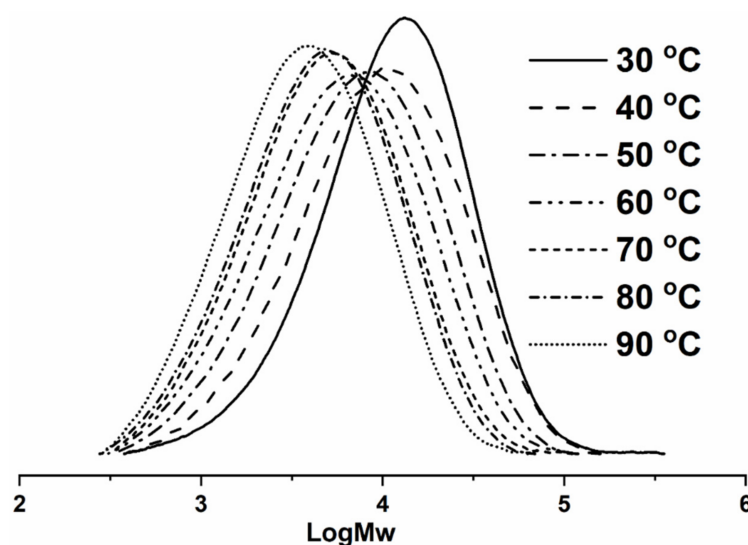
Figure 5. GPC curves showing logM_w of the polyethylenes produced using **Co1**/MAO as a function of the reaction temperature (runs 1–7, Table 2).

Next, the amount of MAO employed was systematically varied by altering the Al:Co molar ratio for **Co1**/MAO from 1500:1 to 3000:1 with the run temperature retained at 70 °C (runs 5, 8–12, Table 2). At 2000:1, the highest catalytic activity of 11.48 × 10^6 g of PE mol^{-1} of Co h^{-1} was achieved (run 5, Table 2), which then declined at higher ratios reaching a low point of 7.47 × 10^6 g of PE mol^{-1} of Co h^{-1} at 3000:1 (run 12, Table 2). In terms of the molecular weight of the polyethylene, the highest value of 7.75 kg mol^{-1} was attained at 1750:1 (run 9, Table 2) and then progressively decreased as the ratio was raised from 2000:1 to 3000:1 (runs 10–12, Table 2). The corresponding GPC curves are given in Figure S3 (Supplementary Materials). It would seem likely that this drop in M_w was due to increased rates in chain transfer and termination reactions in the presence of larger amounts of co-catalyst [48,50,52–55,64–67].

With the Al:Co molar ratio retained at 2000:1 and the temperature set at 70 °C, the time/activity profile of **Co1**/MAO was investigated at selected intervals between 5 and 60 min (runs 5, 13–16, Table 2). Examination of the results indicated an inverse relationship between catalytic activity and run time, with a peak performance observed after 5 min (20.56 × 10^6 g of PE mol^{-1} of Co h^{-1}), which then proceeded to drop-off and reached its lowest value after 60 min (7.01 × 10^6 g of PE mol^{-1} of Co h^{-1}). These results further highlighted the short induction period required to produce the active species (run 13, Table 2) and, moreover, its appreciable lifetime even over longer run times. Meanwhile, the molecular weights of the polyethylenes increased over a prolonged reaction time and remained narrowly dispersed in all cases. The GPC curves of the resulting polyethylenes are collected in Figure S4 (Supplementary Materials).

To explore the influence of ethylene pressure on **Co1**/MAO, the polymerization runs were additionally performed at 5 and 1 atm (runs 5, 17, and 18, Table 2). The results showed a clear correlation between pressure and catalytic activity, as well as the molecular weight of the polyethylene, with higher pressures leading to improved catalytic performance and higher molecular weight polymers. In particular, the catalytic activity displayed at 5 atm of ethylene was almost half that displayed at 10 atm, while the molecular weight of the polyethylene lowered to 6.27 kg mol^{-1} (run 17, Table 2). In comparison, at 1 atm, the catalytic activity dramatically decreased to 0.95 × 10^6 g of PE mol^{-1} of Co h^{-1} while the polymer molecular weight declined to 2.92 kg mol^{-1} (run 18, Table 2). These observations suggested that a high pressure of ethylene was favorable for coordination and insertion, which was likely related to the increased solubility of the ethylene monomer. The GPC curves as a function of ethylene pressure are given in Figure 6.
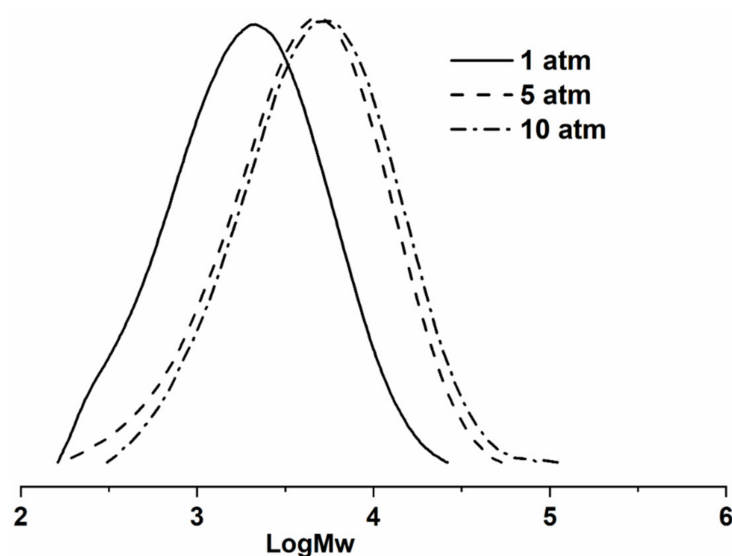
Figure 6. GPC curves showing $\log M_w$ of the polyethylenes produced using **Co1**/MAO as a function of the ethylene pressure (runs 5, 17, and 18, Table 2).

As a general observation for all the different polymerization runs performed using **Co1**/MAO (runs 1–18, Table 2), the polyethylenes showed a narrow dispersity (M_w/M_n range: 2.16 to 2.67; runs 1–18, Table 2), suggesting well-controlled polymerizations as the result of single-site active species.

3.2. Optimization of Polymerization Conditions Using *Co1/MMAO*

With MAO now replaced with MMAO, a similar strategy was employed to optimize the performance of **Co1**/MMAO. The complete set of results are collected in Table 3.

Table 3. Optimization of the polymerization conditions using **Co1**/MMAO [a].

Run	T (°C)	t (min)	Al:Co	PE (g)	Activity [b]	M_w [c]	M_w/M_n [c]	T_m (°C) [d]
1	30	30	2000	1.43	1.91	20.14	2.42	131.2
2	40	30	2000	1.87	2.49	14.36	2.47	130.2
3	50	30	2000	2.54	3.39	11.67	2.54	129.5
4	60	30	2000	3.28	4.37	8.05	2.45	128.2
5	70	30	2000	4.86	6.48	7.28	2.38	128.0
6	80	30	2000	3.72	4.96	6.42	2.25	127.2
7	90	30	2000	1.85	2.47	5.53	2.33	126.4
8	70	30	1500	3.12	4.16	7.60	2.34	127.9
9	70	30	1750	3.97	5.29	7.45	2.31	128.1
10	70	30	2250	5.63	7.51	7.09	2.51	127.9
11	70	30	2500	3.85	5.13	6.64	1.94	128.2
12	70	30	3000	2.74	3.65	3.67	2.45	128.7
13	70	05	2250	2.14	17.12	6.68	2.06	128.0
14	70	15	2250	3.48	9.28	6.90	2.31	127.6
15	70	45	2250	5.92	5.26	7.09	2.10	127.8
16	70	60	2250	6.41	4.27	7.91	2.12	128.0
17 [e]	70	30	2250	2.15	2.87	5.51	2.34	127.7
18 [f]	70	30	2250	0.53	0.71	3.58	1.92	124.1

[a] General conditions: 1.5 μmol of **Co1**, 100 mL toluene, 10 atm C_2H_4, [b] 10^6 g of PE mol^{-1} (Co) h^{-1}, [c] M_w: kg mol^{-1}, determined by GPC, [d] determined by DSC, [e] 5 atm of C_2H_4, [f] 1 atm of C_2H_4.

By running the polymerizations at temperatures between 30 and 90 °C (runs 1–7, Table 3), a peak activity of 6.48×10^6 g of PE mol^{-1} of Co h^{-1} was again observed at 70 °C (run 5, Table 3). However, this activity level was not as high as that observed for **Co1**/MAO at the same temperature. Nonetheless, the optimal temperature of 70 °C again highlighted

the high thermal stability of this class of catalyst [40–46,49,52–57]. At temperatures in excess of 70 °C, the catalytic activity decreased to 4.96×10^6 g of PE mol^{-1} of Co h^{-1} at 80 °C and then to 2.47×10^6 g of PE mol^{-1} of Co h^{-1} at 90 °C (runs 6 and 7, Table 3), highlighting once again the appreciable resilience of the active species to high operating temperature. The molecular weights of the polyethylenes showed a similar trend to that observed with MAO, with the values decreasing from 20.14 to 5.53 kg mol^{-1} when the temperature was raised from 30 to 90 °C (Figure 7). The generated polyethylenes displayed a reasonably narrow dispersity across the temperature range (runs 1–7, Table 3).
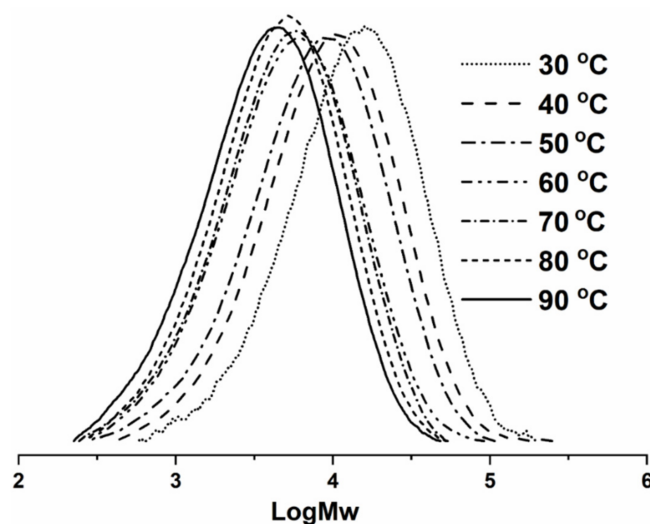

Figure 7. GPC curves showing logM_w of the polyethylenes produced using **Co1**/MMAO as a function of the reaction temperature (runs 1–7, Table 3).

The response of **Co1**/MMAO to variations in Al:Co molar ratio was then explored by altering the ratio from 1500:1 to 3000:1 (runs 5, 8–12, Table 3) with the temperature set at 70 °C. The results revealed a gradual increase in catalytic activity, reaching a maximum of 7.51×10^6 g of PE mol^{-1} of Co h^{-1} at 2250:1 (run 10, Table 4). Further increases in the amount of co-catalyst led to a reduction in activity, with the lowest value of 3.65×10^6 g of PE mol^{-1} of Co h^{-1} obtained at 3000:1 (run 12, Table 3). On the other hand, the molecular weights of the polyethylenes steadily decreased from 7.60 kg mol^{-1} to 3.65 kg mol^{-1} (runs 5, 8–12, Table 3) as the ratio increased (Figure S5 from Supplementary Materials). This finding aligned with increased rates of both chain transfer and termination reactions at higher concentration of co-catalyst [48,50,52–55,64–67].

Table 4. Screening of **Co1**–**Co6** with either MAO or MMAO under optimized conditions [a].

Run	Precat.	Co-Cat.	PE (g)	Activity [b]	M_w [c]	M_w/M_n [c]	T_m (°C) [d]
1	**Co1**	MAO	8.61	11.48	7.40	2.42	127.7
2	**Co2**	MAO	7.03	9.37	13.06	2.54	129.8
3	**Co3**	MAO	3.91	5.21	30.26	2.47	132.9
4	**Co4**	MAO	7.54	10.05	8.10	2.29	128.4
5	**Co5**	MAO	6.88	9.17	13.38	2.53	129.9
6	**Co6**	MAO	2.43	3.24	42.90	2.28	132.8
7	**Co1**	MMAO	5.63	7.51	7.10	2.51	127.9
8	**Co2**	MMAO	3.42	4.56	13.40	2.35	130.0
9	**Co3**	MMAO	2.90	3.87	33.90	1.88	132.7
10	**Co4**	MMAO	5.16	6.88	8.07	2.61	128.0
11	**Co5**	MMAO	3.28	4.37	13.93	2.32	130.0
12	**Co6**	MMAO	2.06	2.74	43.92	2.03	132.4

[a] General conditions: 1.5 μmol of cobalt precatalyst, 100 mL toluene, 10 atm C$_2$H$_4$, 70 °C, 30 min, Al:Co ratio of 2000:1 (MAO) and 2250:1 (MMAO), [b] 10^6 g PE mol^{-1} (Co) h^{-1}, [c] kg mol^{-1} determined by GPC, [d] determined by DSC.

The impact of run time on **Co1**/MMAO was then explored between 5 and 60 min (runs 10, 13–16, Table 3) with the temperature maintained at 70 °C and the Al:Co molar ratio set at 2250:1. Similar to the results observed with MAO, the peak level of 17.12×10^6 g of PE mol^{-1} of Co h^{-1} was found after 5 min (run 13, Table 3). Over a prolonged reaction time, a gradual decrease in catalytic activity was observed, reaching a value of 4.27×10^6 g of PE mol^{-1} of Co h^{-1} after 60 min (runs 16, Table 3). Nonetheless, the levels of activity after longer run times remained appreciable, highlighting the good lifetime of the active species. In terms of the polyethylenes, a gradual increase in molecular weight was observed over time (Figure S6 from Supplementary Materials).

To explore the influence of ethylene pressure on **Co1**/MMAO, we then investigated this parameter using the most effective conditions identified in terms of run temperature and Al:Co molar ratio (runs 10, 17, and 16, Table 3). As with the MAO study, the highest catalytic activity was achieved at the highest pressure of ethylene. At 5 atm, the catalytic activity dropped to 2.87×10^6 g of PE mol^{-1} of Co h^{-1}, while at 1 atm the catalytic activity lowered to 0.71×10^6 g of PE mol^{-1} of Co h^{-1}. Similarly, the molecular weight of the polyethylene dropped to 5.51 kg mol^{-1} at 5 atm (run 17, Table 3) and then fell further to 3.58 kg mol^{-1} at 1 atm (run 18, Table 3). It would seem probable that less effective mass transfer of the ethylene monomer at lower pressure accounted for the observations described above. The GPC curves are given in Figure 8. As a final remark, under all polymerization conditions employed using **Co1**/MMAO, the dispersity of the polyethylenes (M_w/M_n) was in the range 1.92 to 2.54 (runs 1–18, Table 3), indicating the single-site nature of the active species.
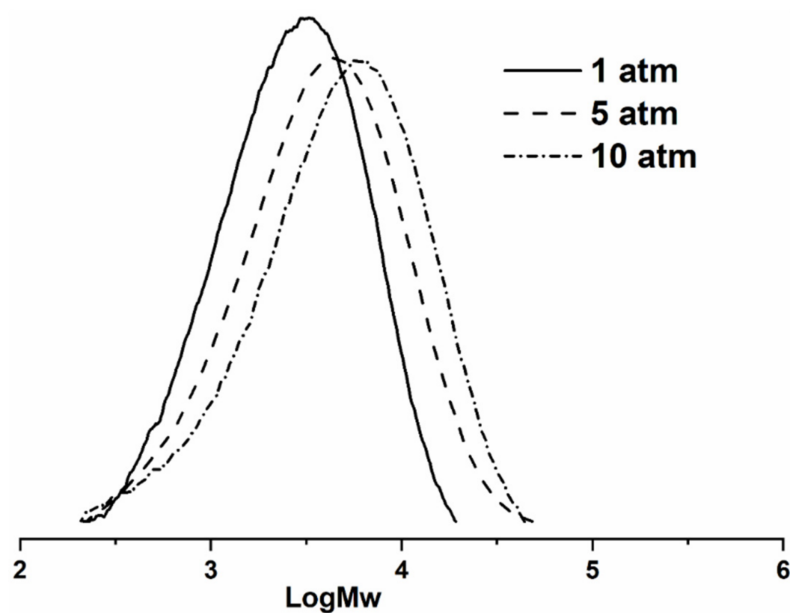

Figure 8. GPC curves showing log M_w of the polyethylenes produced using **Co1**/MMAO as a function of the ethylene pressure (entries 10, 17, and 18, Table 3).

3.3. Screening of *Co1–Co6* with MAO and MMAO

Finally, all the remaining cobalt complexes, **Co2–Co6**, were investigated as precatalysts for ethylene polymerization using the corresponding set of optimized reaction conditions identified with either **Co1**/MAO (reaction temperature = 70 °C, Al:Co molar ratio = 2000:1, run time = 30 min, P_{C2H4} = 10 atm) or **Co1**/MMAO (reaction temperature = 70 °C, Al:Co molar ratio = 2250:1, run time = 30 min, P_{C2H4} = 10 atm). The results are displayed in Table 4.

By utilizing MAO as co-catalyst, all cobalt precatalysts displayed high catalytic activity for ethylene polymerization (range: $3.24–11.48 \times 10^6$ g of PE mol^{-1} of Co h^{-1}) with the relative order following: **Co1** > **Co4** > **Co5** > **Co2** > **Co3** > **Co6** (runs 1–6, Table 4). At

the top end of the range were **Co1** and **Co4,** which both contain the least sterically bulky *ortho*-methyl (R^1) substituents (runs 1, 4, Table 4). Conversely, **Co3,** bearing the bulkier *ortho*-isopropyl substituents, exhibited lower activity, while symmetrical **Co6,** incorporating two *N*-2,4-bis(dibenzosuberyl)-6-fluorophenyl groups, was the least active of the series (runs 3, 6, Table 4). On the other hand, **Co3** and **Co6** generated the highest molecular weight polyethylenes of 30.26 and 42.90 kg mol^{-1}, respectively. Variations in the molecular weight of the polyethylene as a function of precatalyst are shown in Figure 9. These findings suggested that bulkier substituents inhibited chain transfer and protected the active species [42–46,52–57].
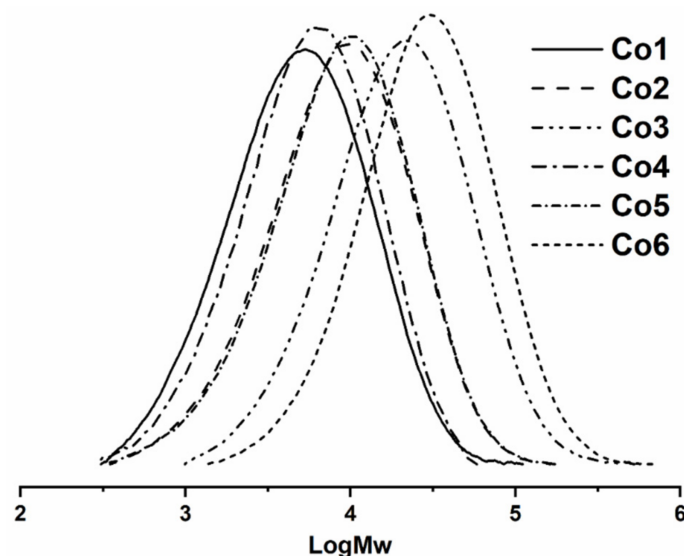

Figure 9. GPC curves showing log M_w of the polyethylenes produced using **Co1**–**Co6** with MAO as activator in each case (runs 1–6, Table 4).

Similarly, using MMAO, the catalytic performance of **Co2**–**Co6** was investigated using the optimum conditions established with **Co1**/MMAO (runs 7–12, Table 4). At first glance, it was evident that the activities for all six cobalt precatalysts mirrored the order observed with MAO: **Co1** > **Co4** > **Co5** > **Co2** > **Co3** > **Co6**. However, these systems generally displayed lower catalytic activities (range: 2.74–7.51 × 10^6 g of PE mol^{-1} of Co h^{-1}), which could plausibly be attributed to the different activation processes involved with each co-catalyst. Nevertheless, steric influences imparted by the *N*-aryl substituents once again played a key role on performance, with the least hindered 2,6-dimethyl **Co1** and **Co4** falling at the top end of the catalytic range (runs 7, 10, Table 4). Likewise, the highest molecular weight polyethylene was generated using the bulkiest precatalysts, **Co6** (M_w = 43.93 kg mol^{-1}) and **Co3** (M_w = 33.90 kg mol^{-1}) (runs 9, 12, Table 4). The GPC curves of the polyethylenes generated using **Co1**–**Co6**/MMAO are shown in Figure 10. As was noted in the initial studies using **Co1**/MAO or **Co1**/MMAO, the polymers produced using **Co1**–**Co6** were narrowly dispersed, with M_w/M_n values falling in the range of 1.88 to 2.61, highlighting the good control and single-site nature of the active species.
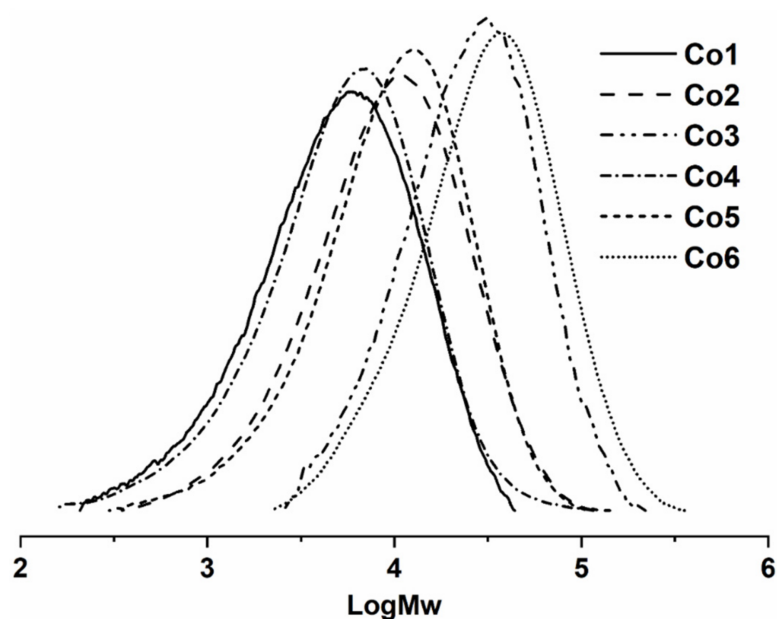
Figure 10. GPC curves showing $\log M_w$ of the polyethylenes produced using **Co1**–**Co6** with MMAO as activator in each case (runs 7–12, Table 4).

3.4. Microstructural Features of the Polyethylenes

As is apparent from Tables 2–4, all of the polyethylene samples produced in this work displayed melting points (T_m) in the range 126.1–132.9 °C, values that are typical of linear polyethylenes. Indeed, bis(imino)pyridine-cobalt catalysts have a history for forming polymers with very little branching [1–6,60,64–71]. To investigate the structural composition of these polyethylenes in more detail, selected samples generated using the more active catalysts that were activated using MAO and MMAO, were investigated using ^{1}H and ^{13}C NMR spectroscopy. To allow suitable solubility, these samples were dissolved in deuterated $C_2D_2Cl_4$ at high temperature and their spectra were recorded at 100 °C.

Firstly, a sample obtained using **Co1**/MAO at the optimal temperature of 70 °C (M_w = 7.40 kg mol^{-1}, run 5, Table 2) was recorded and analyzed using approaches detailed in the literature [36,45–48,52–59,68–71]. The ^{1}H NMR spectrum displayed characteristic peaks for a vinyl-terminated polyethylene displaying high linearity (Figure 11). In particular, a high intensity singlet at δ 1.30 ppm for the –$(CH_2)_n$– repeat unit was observed along with two less intense downfield multiplets at δ 5.91 and δ 4.98 ppm in a 1:2 intensity ratio, which was assigned to the vinyl end group (–CH=CH$_2$). In addition, a weak signal for the protons on the carbon adjacent to vinyl group (H_c) were visible more upfield at δ 2.12 ppm, while the protons belonging to methyl end group (H_f) were detected most upfield at δ 0.98 ppm. On the other hand, signals for H_e and H_f could not be observed and were presumably masked by the signal for –$(CH_2)_n$– repeat unit, while H_d could be just identified at δ 1.54 ppm.

In the ^{13}C NMR spectrum of this polyethylene sample (Figure 12), the signal for the –$(CH_2)_n$– repeat unit took the form of an intense resonance at δ 30.00 ppm. On either side of this peak, weaker signals for the methylene carbons, C_c, C_d, and C_f, could be detected, with the methyl chain end observed most upfield at δ 14.2 ppm. Conversely, the vinylic carbons, C_b and C_a were found most downfield at δ 139.61 and 114.39 ppm, whereas the signal for the carbon atom C_c adjacent to this vinyl end group appeared at δ 33.98 ppm. Notably, the integral ratio of the methyl and vinyl end (C_g:C_a) in ^{13}C NMR spectrum was found to be approximately 1:1, which provided support for a vinyl-terminated polymer. Overall, this observation of a vinyl end group in both the ^{1}H NMR and ^{13}C NMR spectra implied that β-hydrogen elimination represented the termination pathway in this polymerization process [50–53,70,71].
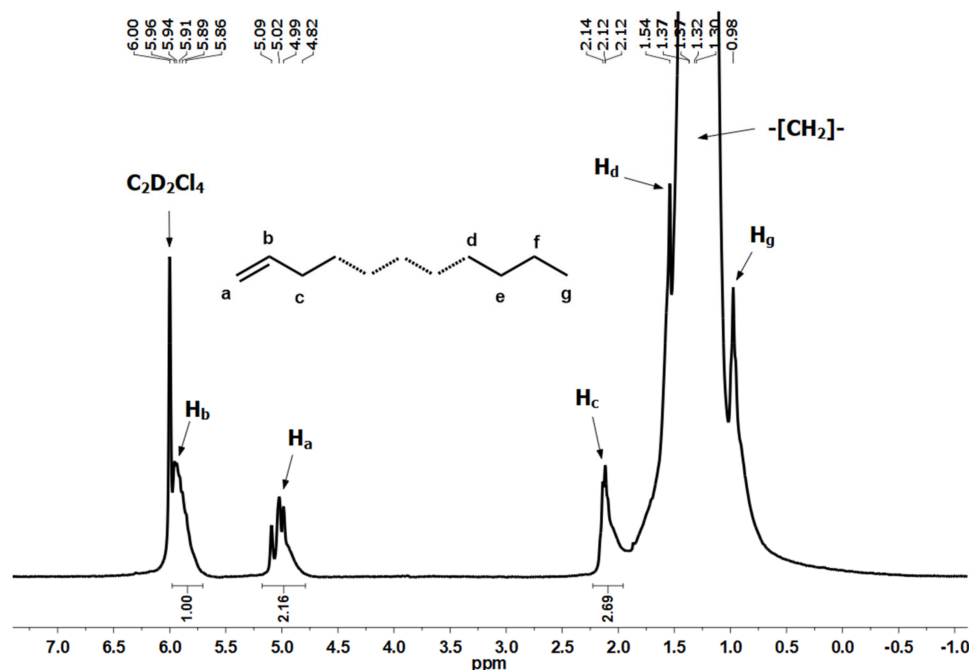
Figure 11. ^{1}H NMR spectrum of the polyethylene generated using **Co1**/MAO (run 5, Table 2); recorded in $C_2D_2Cl_4$ at 100 °C.

A similar analysis was performed on the ^{1}H and ^{13}C NMR spectra of the polyethylene afforded using **Co1**/MMAO at 70 °C (M_w = 7.09 kg mol^{-1}, run 10, Table 3). As was noted above, signals characteristic of a vinyl-terminated polyethylene with high linearity were evident (Figures S7 and S8 from Supplementary Materials) [36,45–48,52–59,68–71]. Clearly, β-hydrogen elimination again accounted for the key termination pathway when using MMAO as co-catalyst.
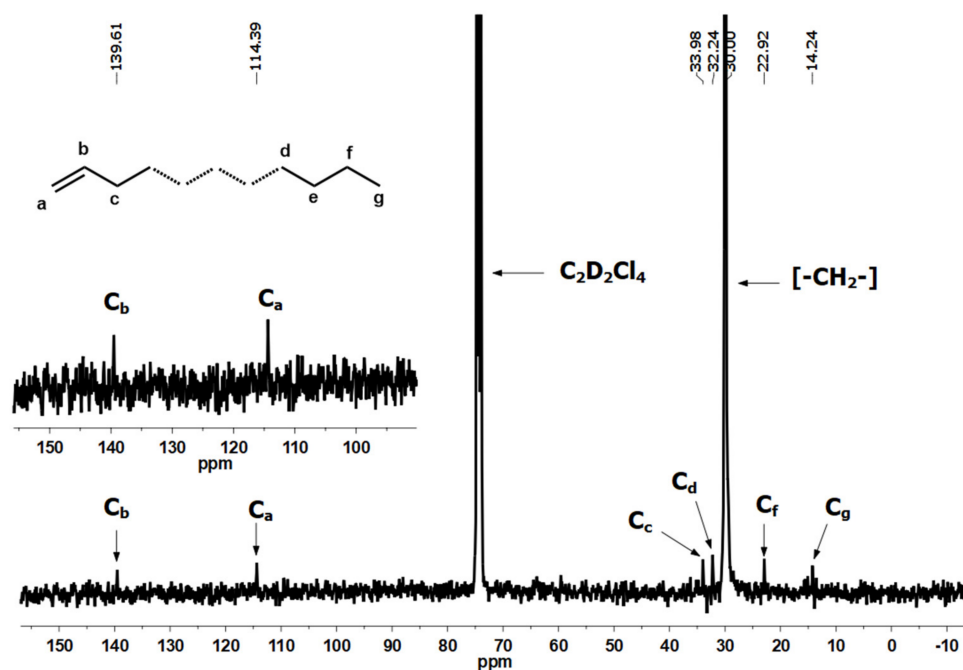

Figure 12. ^{13}C NMR spectrum of the polyethylene generated using **Co1**/MAO (run 5, Table 2); recorded in $C_2D_2Cl_4$ at 100 °C.

3.5. Comparative Study of the Current Catalyst System with Previously Reported Examples

To facilitate a comparison of the current class of precatalysts with related unsymmetrical cobalt(II) chloride precatalysts [36,37,48,52,54], Figure 13 presents various performance data for previously reported **B–F** alongside that for **G**. All the tests were carried out under optimal reaction conditions at P_{C2H4} = 10 atm using MAO as the co-catalyst.
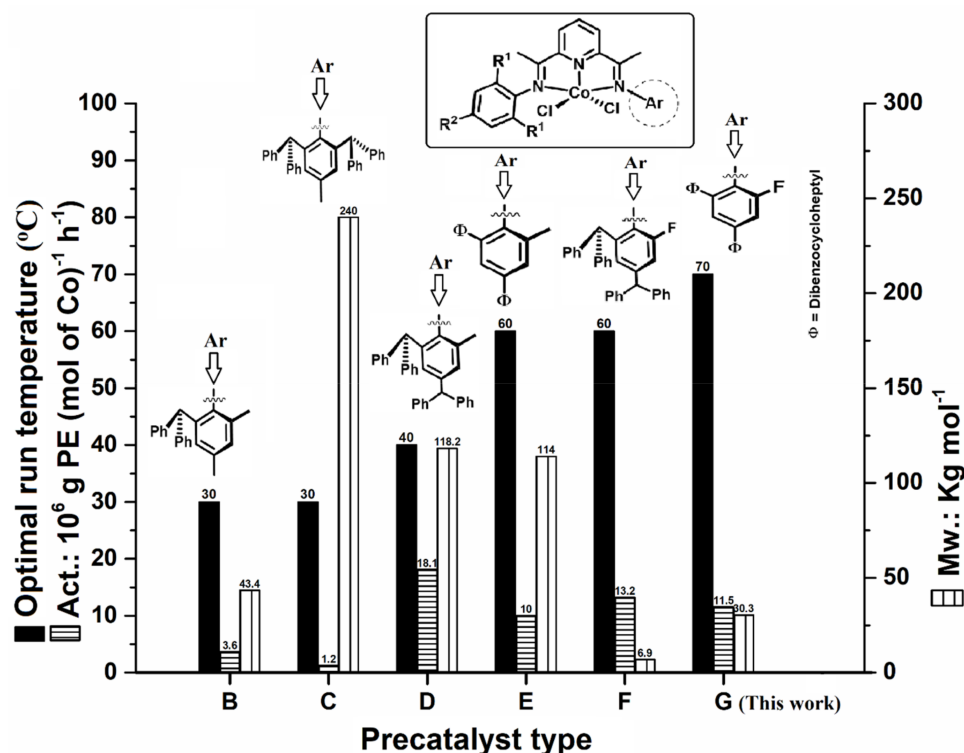

Figure 13. Comparison of catalytic activity, optimal run temperature, and polymer molecular weight data for **G** (this work) with that obtained using **B–F**. All runs were performed under optimized conditions at 10 atm of C_2H_4 using MAO as the activator.

Several notable findings emerged from inspection of the figure. Firstly, the highest optimal run temperature was displayed by **G** (70 °C); for **B–F** this temperature fell anywhere between 30 and 60 °C. This observation lent support for the beneficial effect of the introduction of a *N*-2,4-bis(dibenzosuberyl)-6-fluorophenyl group on the thermal stability of the cobalt catalyst. In terms of catalytic activity, **G** (11.5 × 10^6 g of PE mol^{-1} (Co) h^{-1}) was the third most active system, with only **D** [48] and **F** exceeding it under optimal operating conditions. Nonetheless, **G** was more active than **B** [36], **C** [37], and **E** [52], as well as several other reported precatalysts bearing *N*-aryl substituents appended with electron withdrawing/donating groups in combination with benzhydryl groups [39–42,45]. Evidently, the presence of the *N*-2,4-bis(dibenzosuberyl)-6-fluorophenyl group did not significantly enhance activity. In terms of the molecular weight of the polyethylene, that generated with **G** (30.3 kg/mol) was higher than that with **F** [54], although less than that produced using **B–E**. However, it would seem most likely that this relatively low molecular weight polymer was due to the higher run temperature leading to a higher rate of chain transfer compared to **B–E**.

4. Experimental

4.1. General Considerations

Manipulations of all air and/or moisture sensitive compounds were undertaken using standard Schlenk techniques under inert nitrogen atmosphere conditions. All solvents prior to use were distilled under nitrogen. The aluminum-alkyls, methylaluminoxane

(MAO, 1.46 M in toluene), and modified-methylaluminoxane (MMAO, 1.93 M in *n*-heptane) were purchased from Akzo Nobel Corp. (Nanjing, China), while the high-purity ethylene was bought from Beijing Yanshan Petrochemical Co. (Beijing, China). All other reagents were purchased from either Aldrich (Beijing, China) or Acros (Beijing, China). The *N*-2,4-bis(dibenzosuberyl)-6-fluoroaniline was prepared according to a described procedure [52,53,58,59]. The ^{1}H, ^{13}C, and ^{19}F NMR spectra of all bis(imino)pyridines and their precursors were recorded on a Bruker DMX 400M Hz NMR (Bruker, Karlsruhe, Germany) at ambient temperature using TMS as an internal standard. The FT-IR spectra were recorded on the Perkin Elmer Spectrum 2000 FT-IR spectrometer (Shanghai, China). The elemental analyses were carried out on a Flash EA 1112 microanalyzer (Thermo Electron SPA, Beijing, China). The molecular weight (M_w) and dispersity (M_w/M_n) of the polyethylenes were measured using a PL-GPC 220 instrument (PL, Shropshire, UK) operating at 150 °C and using 1,2,4-trichlorobenzene as the eluting solvent. The melting points of the polyethylenes were measured using differential scanning calorimetry (Q2000 DSC; TA Instruments, New Castle, DE, USA) under a nitrogen atmosphere. Typically, a PE sample of 5.0 mg was heated to 160 °C at a heating rate of 20 °C min^{-1} and maintained for 3 min at the same temperature to remove its thermal history. This sample was then cooled to −20 °C at a rate of 20 °C min^{-1}. The ^{1}H and ^{13}C NMR spectra of the polyethylenes were recorded in deuterated 1,1,2,2-tetrachloroethane at 100 °C. Sample preparation typically involved taking a known amount of polyethylene (90–100 mg) and dissolving it in deuterated 1,1,2,2-tetrachloroethane (2.0 mL) at high temperature before an aliquot was transferred to a 5 mm standard glass NMR tube. Inverse-gated ^{13}C NMR spectra were recorded on a Bruker DMX 300 MHz spectrometer (Bruker) with the number of scans anywhere between 1798 and 1935. The conditions used for the spectral analysis were as follows: a spectral width of 22675.7 kHz, acquisition time of 0.7225 s, relaxation delay of 5.0 s, and pulse width of 15.5 μs.

4.2. Synthesis of 2-{(2,4-(C$_{15}$H$_{13}$)$_2$-6-FC$_6$H$_2$)N=CMe}-6-(O=CMe)C$_5$H$_3$N

To a round-bottom flask containing 2,6-diacetylpyridine (3.30 g, 20.2 mmol) in toluene (100 mL) was added 2,4-bis(dibenzosuberyl)-6-fluoroaniline (10.02 g, 20.2 mmol), before a Dean-Stark trap was fitted. The reaction mixture was stirred under reflux for 10 min and then a catalytic amount of *p*-toluenesulfonic acid (ca. 15 mol%) was slowly added. After a further 6 h under reflux, the reaction mixture was allowed to cool to room temperature, at which point all volatiles were evaporated under reduced pressure. The resulting residue was then purified by column chromatography (on basic alumina) using an eluent composed of petroleum ether and diethyl ether (25:2) to afford the title compound as a pale yellow solid (4.36 g, 34%). Mp: 203–205 °C. ^{1}H NMR (400 MHz, CDCl$_3$, TMS): δ 8.52 (d, *J* = 7.9 Hz, Py–H, 1H), 8.13 (d, *J* = 7.7 Hz, Py–H, 1H), 7.97 (t, *J* = 7.8 Hz, Py–H, 1H), 7.26–6.85 (m, Ar–H, 14H), 6.58 (s, Ar–H$_m$, 1H), 6.32 (d, *J* = 11.2 Hz, Ar–H, 2H), 6.12 (s, Ar–H$_m$, 1H), 5.16 (s, –CH–, 1H), 4.98 (s, –CH–, 1H), 3.02–2.86 (m, –CH$_2$–, 3H), 2.81 (s, –CH$_3$, 3H), 2.80–2.72 (m, –CH$_2$–, 5H), 1.63 (s, –CH$_3$, 3H). ^{13}C NMR (100 MHz, CDCl$_3$, TMS): δ 200.2, 170.7, 155.1, 152.3, 140.8, 140.7, 139.8, 137.1, 135.0, 134.0, 131.3, 130.6, 127.3, 126.7, 126.1, 125.7, 125.0, 122.5, 112.6, 112.4, 57.7, 56.2, 32.3, 25.7, 16.2. TMS FT-IR (KBr cm^{-1}): 3051 (w), 3060 (w), 3012 (w), 2926 (w), 2836 (w), 2829 (w), 1704 (υ(C=O), s), 1649 (υ(C=N), s), 1584 (w), 1528 (w), 1491 (m), 1463 (w), 1429 (w), 1364 (s), 1309 (m), 1234 (m), 1150 (w), 1120 (w), 1078 (w), 1042 (w), 1014 (w), 990 (w), 940 (w), 892 (w), 828 (w), 816 (m), 790 (w), 760 (s), 734 (m), 701 (m), 668 (w).

*4.3. Synthesis of 2-{(2,4-(C$_{15}$H$_{13}$)$_2$-6-FC$_6$H$_2$)N=CMe}-6-(ArN=CMe)C$_5$H$_3$N (**L1–L5**)*
4.3.1. Ar = 2,6-Me$_2$C$_6$H$_3$ (**L1**)

A mixture of the imine-ketone 2-{(2,4-(C$_{15}$H$_{13}$)$_2$-6-FC$_6$H$_2$)N=CMe}-6-(O=CMe)C$_5$H$_3$N (1.01 g, 1.58 mmol) and 2,6-dimethylaniline (0.25 g, 2.06 mmol), along with a catalytic amount of *p*-toluenesulfonic acid (ca. 15%) in toluene, were loaded into a round-bottom flask equipped with a Dean-Stark trap. The reaction mixture was stirred under reflux for

6 h and then allowed to cool to room temperature before all volatiles were removed under reduced pressure. The resulting residue was purified by column chromatography (using basic alumina) using a mixture of petroleum ether and diethyl ether (25:2) as the eluent to give **L1** as a yellow powder (0.68 g, 8%). Mp: 254–256 °C. ^{1}H NMR (400 MHz, CDCl$_3$, TMS): δ 8.47 (d, *J* = 7.6 Hz, Py–H, 1H), 8.42 (d, *J* = 8.0 Hz, Py–H, 1H), 7.94 (t, *J* = 7.8 Hz, Py–H, 1H), 7.22–7.06 (m, Ar–H, 19H), 6.52 (d, *J* = 11.2 Hz, Aryl–H, 1H), 6.36 (s, aryl–H$_m$, 1H), 5.13 (s, –CH–, 1H), 5.09 (s, –CH–, 1H), 3.01–2.93 (m, –CH$_2$–, 3H), 2.83–2.79 (m, –CH$_2$–, 1H), 2.70–2.62 (m, –CH$_2$–, 3H), 2.52–2.48 (m, –CH$_2$–, 1H), 2.18 (s, –CH$_3$, 3H), 2.08 (s, –CH$_3$, 6H), 1.67 (s, –CH$_3$, 3H). ^{13}C NMR (100 MHz, CDCl$_3$, TMS): δ 171.3, 167.3, 155.0, 154.7, 151.8, 149.4, 148.8, 140.6, 140.5, 140.1, 140.0, 139.8, 139.1, 136.7, 135.0, 134.4, 134.3, 131.4, 131.2, 131.0, 130.6, 130.1, 127.9, 127.3, 127.2, 127.1, 126.9, 126.3, 126.1, 126.0, 125.7, 125.5, 123.0, 122.7, 122.2, 112.6, 112.4, 57.7, 57.4, 56.2, 32.3, 31.3, 18.0, 16.4. ^{19}F NMR (470 MHz, CDCl$_3$): δ –128.68. FT-IR (KBr cm^{-1}): 3060 (w), 3022 (w), 2930 (w), 2889 (w), 2827 (w), 1645 (υ(C=N), s), 1581 (w), 1493 (w), 1452 (m), 1360 (s), 1301 (w), 1247 (w), 1202 (m), 1130 (m), 1101(w), 1050 (w), 1021 (w), 994 (w), 961 (w), 934 (w), 872 (w), 8061 (m), 771 (s), 718 (m), 687 (w). Anal. Calcd. for C$_{53}$H$_{46}$N$_3$F·0.5H$_2$O (752.98): C, 84.54; H, 6.29; N, 5.58. Found: C, 84.60; H, 6.29; N, 5.37.

4.3.2. Ar = 2,6-Et$_2$C$_6$H$_3$ (**L2**)

Using a similar procedure as described for the synthesis of **L1**, **L2** was prepared as a yellow powder (0.34 g, 26%). Mp: 212–214 °C. ^{1}H NMR (400 MHz, CDCl$_3$, TMS): ^{1}H NMR (400 MHz, CDCl$_3$, TMS): δ 8.45 (d, *J* = 8.0 Hz, Py–H, 1H), 8.42 (d, *J* = 8.0 Hz, Py–H, 1H), 7.94 (t, *J* = 7.8 Hz, Py–H, 1H), 7.22–7.09 (m, Ar–H, 17H), 7.20 (Ar–H$_m$, 1H), 6.87 (d, *J* = 11.2 Hz, Ar–H, 2H), 6.36 (s, Aryl–H$_m$, 1H), 5.12 (s, –CH–, 1H), 5.08 (s, –CH–, 1H), 3.00–2.95 (m, –CH$_2$–, 3H), 2.70–2.56 (m, –CH$_2$–, 4H), 2.74–2.34 (m, –CH$_2$–, 5H), 2.19 (s, –CH$_3$, 3H), 1.61 (s, –CH$_3$, 3H), 1.17 (t, *J* = 7.4 Hz, –CH$_3$, 6H). ^{13}C NMR (100 MHz, CDCl$_3$, TMS): δ 171.3, 167.0, 155.0, 154.7, 151.8, 149.4, 147.8, 140.6, 140.5, 139.8, 136.7, 135.0, 134.4, 134.3, 131.5, 131.2, 127.3, 126.7, 126.1, 126.0, 125.8, 123.3, 122.7, 122.2, 112.6, 112.4, 57.7, 56.2, 32.3, 24.6, 16.8, 16.4, 16.3, 13.8. ^{19}F NMR (470 MHz, CDCl$_3$): δ –128.64. FT-IR (KBr cm^{-1}): 3060 (w), 3010 (w), 2956 (m), 2922 (w), 2854 (w), 1650 (υ(C=N), s), 1580 (w), 1554 (w), 1510 (w), 1481(w), 1443 (m), 1427 (m), 1382 (w), 1357 (m), 1319 (w), 1304 (w), 1241 (w), 1217 (w), 1188 (w), 1116 (m), 1081 (w), 1049 (w), 1016 (w), 961 (w), 924 (w), 886 (w), 840 (w), 772 (w), 762 (m), 736 (s), 712 (w), 662 (w). Anal. Calcd. for C$_{55}$H$_{50}$N$_3$F·0.5H$_2$O (781.03): C, 84.58; H, 6.58; N, 5.38. Found: C, 84.77; H, 6.59; N, 5.04.

4.3.3. Ar = 2,6-*i*-Pr$_2$C$_6$H$_3$ (**L3**)

Using a similar procedure as described for the synthesis of **L1**, **L3** was prepared as a yellow powder (0.38 g, 28%). Mp: 243–245 °C. ^{1}H NMR (400 MHz, CDCl$_3$, TMS): δ 8.45 (d, *J* = 7.6 Hz, Py–H, 1H), 8.41 (d, *J* = 7.6 Hz, Py–H, 1H), 7.95 (t, *J* = 8.0 Hz, Py–H, 1H), 7.22–7.00 (m, Py–H, 17H), 6.88 (d, *J* = 7.2 Hz, Ar–H, 1H), 6.46 (s, Ar–H$_m$, 1H), 6.25 (d, *J* = 11.2 Hz, Ar–H, 1H), 6.36 (s, Ar–H$_m$, 1H), 5.12 (s, –CH–, 1H), 5.09 (s, –CH– 1H), 3.01–2.95 (m, –CH$_2$–, 3H), 2.80–2.70 (m, –CH$_2$–, 5H), 2.52–2.36 (m, –CH–, 2H), 2.21 (s, –CH$_3$, 3H), 1.68 (s, –CH$_3$, 3H), 1.19 (t, *J* = 6.4 Hz, –CH$_3$, 12H). ^{13}C NMR (100 MHz, CDCl$_3$, TMS): δ 171.3, 167.1, 155.0, 154.7, 146.7, 140.5, 139.8, 136.6, 135.8, 135.0, 134.4, 131.4, 127.2, 126.6, 126.1, 125.6, 123.6, 123.0, 122.6, 122.2, 112.5, 112.3, 57.6, 56.1, 32.2, 28.3, 23.2, 22.9, 17.1, 16.4. ^{19}F NMR (470 MHz, CDCl$_3$): δ –128.69. FT-IR (KBr cm^{-1}): 3058 (w), 3008 (w), 2957(m), 2918 (w), 2862 (w), 1651 (υ(C=N), s), 1588 (w), 1564 (w), 1512 (w), 1491(w), 1448 (m), 1429 (w), 1392 (w), 1359 (m), 1321(w), 1301 (w), 1239 (w), 1219 (w), 1191 (w), 1156 (w), 1114 (m), 1078 (w), 1046 (w), 1013 (w), 957 (w), 928 (w), 895 (w), 844 (w), 817 (w), 778 (w), 765 (m), 751 (s), 741 (s), 717 (w), 682 (w). Anal. Calcd. for C$_{57}$H$_{54}$N$_3$F·0.5H$_2$O (809.09): C, 84.62; H, 6.85; N, 5.19. Found: C, 84.50; H, 6.88; N, 5.51.

4.3.4. Ar = 2,4,6-Me$_3$C$_6$H$_2$ (L4)

Using a similar procedure as described for the synthesis of **L1**, **L4** was prepared as a yellow powder (0.42 g, 32%). Mp: 217–219 °C. ^{1}H NMR (400 MHz, CDCl$_3$, TMS): δ 8.46 (d, J = 7.6 Hz, Py–H, 1H), 8.42 (d, J = 8.0 Hz, Py–H, 1H), 7.94 (t, J = 7.8 Hz, Py–H, 1H), 7.22–6.91 (m, Ar–H, 16H), 6.87 (d, J = 7.6 Hz, Ar–H, 1H), 6.96 (s, Ar–H$_m$, 1H), 6.52 (d, J = 11.2 Hz, Ar–H, 1H), 6.36 (s, Ar–H$_m$, 1H), 5.12 (s, –CH–, 1H), 5.09 (s, –CH–, 1H), 3.01–2.96 (m, –CH$_2$–, 3H), 2.83–2.47 (m, –CH$_2$–, 5H), 2.31 (s, –CH$_3$, 3H), 2.18 (s, –CH$_3$, 3H), 2.04 (s, –CH$_3$, 6H), 1.67 (s, –CH$_3$, 3H). ^{13}C NMR (100 MHz, CDCl$_3$, TMS): δ 171.3, 167.5, 155.1, 154.6, 151.8, 149.4, 147.8, 146.3, 140.6, 140.5, 139.8, 136.6, 135.0, 134.4, 134.3, 132.2, 131.4, 131.2, 130.6, 128.6, 127.3, 127.1, 126.7, 126.1, 125.7, 125.3, 122.7, 122.2, 112.6, 112.4, 57.7, 56.2, 32.3, 31.3, 20.8, 17.9, 16.4. ^{19}F NMR (470 MHz, CDCl$_3$): δ –128.67. FT-IR (KBr cm^{-1}): 3060 (w), 3014 (w), 2963 (w), 2894 (w), 2860 (w), 1644 (υ(C=N), s), 1576 (w), 1542 (w), 1491 (s), 1447 (w), 1428 (w), 1386 (w), 1351 (m), 1293 (w), 1256 (w), 1221 (s), 1192 (w), 1124 (m), 1078 (w), 1045 (w), 1011 (w), 981 (w), 938 (w), 890 (w), 848 (s), 809 (w), 755 (s), 710 (w), 682 (w). Anal. Calcd. for C$_{54}$H$_{48}$N$_3$F·0.5H$_2$O (767.00): C, 84.56; H, 6.44; N, 5.48. Found: C, 84.47; H, 6.54; N, 5.16.

4.3.5. Ar = 2,6-Et$_2$-4-MeC$_6$H$_2$ (L5)

Using a similar procedure as described for the synthesis of **L1**, **L5** was prepared as a yellow powder (0.75 g, 54%). Mp: 234–236 °C. ^{1}H NMR (400 MHz, CDCl$_3$, TMS): δ 8.44 (d, J = 8.0 Hz, Py–H, 1H), 8.41 (d, J = 7.6 Hz, Py–H, 1H), 7.93 (t, J = 7.8 Hz, Py–H, 1H), 7.20–6.94 (m, Ar–H, 16H), 6.87 (s, Ar–H$_m$, 1H), 6.51 (d, J = 10.8 Hz, Ar–H, 2H), 6.36 (s, Ar–H$_m$, 1H), 5.11 (s, –CH–, 1H), 5.08 (s, –CH–, 1H), 3.01–2.95 (m, –CH$_2$–, 3H), 2.69–2.49 (m, –CH$_2$–, 5H), 2.43–2.40 (m, –CH$_2$–, 4H), 2.38 (s, –CH$_3$, 3H), 2.18 (s, –CH$_3$, 3H), 1.66 (s, –CH$_3$, 3H), 1.15 (t, J = 7.2 Hz, –CH$_3$, 6H). ^{13}C NMR (100 MHz, CDCl$_3$, TMS): δ 171.3, 167.2, 155.2, 154.5, 145.3, 140.5, 139.8, 136.6, 135.0, 134.3, 132.4, 131.5, 131.1, 130.8, 127.3, 126.7, 126.6, 126.1, 125.7, 122.6, 122.2, 112.6, 112.4, 57.7, 56.2, 32.2, 24.6, 21.0, 16.8, 16.4, 13.9. ^{19}F NMR (470 MHz, CDCl$_3$): δ –128.68. FT-IR (KBr cm^{-1}): 3026 (w), 2966 (w), 2941 (w), 2870 (w), 2829 (w) 1648 (υ(C=N), s), 1579 (w), 1526 (w), 1490 (w), 1461 (s), 1418 (w), 1411 (w), 1356 (m), 1329 (w), 1305 (w), 1283 (w), 1240 (w), 1211 (s), 1180 (w), 1138 (w), 1114 (m), 1068 (w), 1034 (w), 992 (w), 938 (w), 908 (w), 892 (w), 854 (s), 826 (m), 784 (m), 756 (s), 714 (w), 667 (w). Anal. Calcd. for C$_{56}$H$_{52}$N$_3$F·1.5H$_2$O (813.07): C, 82.73; H, 6.82; N, 5.17. Found: C, 82.50; H, 6.83; N, 4.94.

4.4. Synthesis of 2,6-{(2,4-(C$_{15}$H$_{13}$)$_2$-6-FC$_6$H$_2$)N=CMe}$_2$C$_5$H$_3$N (*L6*)

During the chromatographic purification process used to isolate the imine-ketone 2-{(2,4-(C$_{15}$H$_{13}$)$_2$-6-FC$_6$H$_2$)N=CMe}-6-(O=CMe)C$_5$H$_3$N (see above), a second fraction was removed from the column that was identified as bis(imino)pyridine **L6** and isolated as a pale yellow solid (3.24 g, 14%). Mp: 204–206 °C. ^{1}H NMR (400 MHz, CDCl$_3$, TMS): δ 8.44 (d, J = 8.0 Hz, Py–H, 2H), 7.98 (t, J = 8.00 Hz, Py–H, 1H), 7.21–7.01 (m, Ar–H, 26H), 6.80 (d, J = 4.0 Hz, Ar–H, 6H), 6.51 (Ar–H$_m$, 2H), 6.34 (s, Ar–H$_m$, 2H), 5.08 (s, –CH–, 2H), 3.00–2.94 (m, –CH$_2$–, 5H), 2.72–2.68 (m, –CH$_2$–, 8H), 2.45–2.21 (m, –CH$_2$–, 3H), 1.55 (s, –CH$_3$, 6H). ^{13}C NMR (100 MHz, CDCl$_3$, TMS): δ 171.4, 154.5, 151.8, 149.4, 140.6, 140.5, 140.1, 140.0, 139.8, 136.4, 135.1, 134.4, 134.2, 131.4, 131.2, 131.0, 130.6, 130.1, 129.1, 128.3, 127.3, 127.1, 126.7, 126.3, 126.1, 126.0, 125.7, 122.7, 112.6, 112.3, 57.7, 56.2, 32.3, 31.3, 16.4, 16.3. ^{19}F NMR (470 MHz, CDCl$_3$): δ –128.66. FT-IR (KBr cm^{-1}): 3026 (w), 2966 (w), 2941 (w), 2870 (w), 2829 (w) 1650 (υ(C=N), s), 1576 (w), 1536 (w), 1472 (w), 1452 (m), 1412 (w), 1356 (s), 1320 (w), 1301 (w), 1244 (w), 1228 (w), 1201 (m), 1176 (w), 1125 (m), 1056 (w), 1014 (w), 982 (w), 918 (w), 872 (w), 834 (m), 764 (m), 750 (s), 714 (w), 670 (w). Anal. Calcd. for C$_{81}$H$_{65}$N$_3$F$_2$·0.5H$_2$O (1126.52): C, 86.29; H, 5.90; N, 3.73. Found: C, 86.40; H, 5.68; N, 3.80.

4.5. Synthesis of [2-{(2,4-(C$_{15}$H$_{13}$)$_2$-6-FC$_6$H$_2$)N=CMe}-6-(ArN=CMe)C$_5$H$_3$N]CoCl$_2$ (*Co1–Co6*)
4.5.1. Ar = 2,6-Me$_2$C$_6$H$_3$ (**Co1**)

To a Schlenk tube containing **L1** (0.20 g, 0.27 mmol) and anhydrous CoCl$_2$ (0.035 g, 0.27 mmol) was added dichloromethane (5 mL) and ethanol (5 mL). The reaction mixture

was stirred at room temperature for 12 h. All volatiles were then removed under reduced pressure and an excess of diethyl ether added to induce precipitation. The precipitate was filtered, washed with more diethyl ether (3 × 15 mL), and dried to afford **Co1** as a green powder (0.15 g, 62%). FT-IR (KBr cm^{-1}): 3057 (w), 3016 (w), 2926 (w), 2883 (w), 2828 (w), 1625 (υ(C=N), m), 1587 (s), 1572 (m), 1492 (m), 1471 (m), 1444 (m), 1421 (s), 1370 (m), 1310 (w), 1261 (s), 1215 (m), 1184 (w), 1162 (w), 1120 (w), 1045 (w), 1027 (w), 995 (w), 946 (w), 922 (w), 876 (w), 841 (w), 814 (m), 785 (w), 765 (s), 706 (m), 683 (w). ^{19}F NMR (470 MHz, CDCl$_3$): δ −146.68. Anal. Calcd. for C$_{53}$H$_{46}$Cl$_2$CoN$_3$F·EtOH (919.87): C, 71.81; H, 5.70; N, 4.57. Found: C, 75.23; H, 5.73; N, 4.86.

4.5.2. Ar = 2,6-Et$_2$C$_6$H$_3$ (**Co2**)

Using the same procedure and molar ratios as described for **Co1**, **Co2** was isolated as a green powder (0.14 g, 58%). FT-IR (KBr cm^{-1}): 3064 (w), 3016 (w), 2965 (w), 2930 (w), 2878 (w), 2834 (w), 1623 (υ(C=N), m), 1588 (s),1571 (w), 1492 (m), 1470 (m), 1445 (s), 1420 (w), 1371 (m), 1312 (w), 1261 (s), 1214 (m), 1204 (w), 1169 (w), 1102 (w), 1061 (w), 1047 (w), 1028 (w), 999 (w), 949 (w), 916 (w), 879 (w), 841 (w), 809 (m), 791 (w), 769 (s),755 (s), 742 (m), 716 (w). ^{19}F NMR (470 MHz, CDCl$_3$): δ −141.96. Anal. Calcd, for C$_{55}$H$_{50}$Cl$_2$CoN$_3$F (901.86): C, 73.25; H, 5.59; N, 4.66. Found: C, 72.99; H, 5.50; N, 4.67.

4.5.3. Ar = 2,6-*i*-Pr$_2$C$_6$H$_3$ (**Co3**)

Using the same procedure and molar ratios as described for **Co1**, **Co3** was isolated as a green powder (0.13 g, 54%). FT-IR (KBr cm^{-1}): 3060 (w), 3016 (w), 2963 (w), 2928 (w), 2867 (w), 1623 (υ(C=N), m), 1591 (m), 1568 (m), 1561 (w), 1496 (s), 1465 (w), 1441 (w), 1418 (s), 1384 (w), 1370 (s), 1314 (m), 1201 (w), 1184 (w), 1162 (w), 1101 (w), 1061 (w), 1046 (w), 1026 (w), 991 (w), 978 (w), 938 (w), 878 (w), 843 (w), 813 (w), 797 (w), 785 (w), 769 (s), 760 (m), 742 (w). ^{19}F NMR (470 MHz, CDCl$_3$): δ –129.32. Anal. Calcd, for C$_{57}$H$_{54}$Cl$_2$CoN$_3$F·EtOH (975.98): C, 72.61; H, 6.20; N, 4.31. Found: C, 72.60; H, 5.86; N, 4.43.

4.5.4. Ar = 2,4,6-Me$_3$C$_6$H$_2$ (**Co4**)

Using the same procedure and molar ratios as described for **Co1**, **Co4** was isolated as a green powder (0.16 g, 70%). FT-IR (KBr cm^{-1}): 3058 (w), 3011 (w), 2959 (w), 2921 (w), 2864 (w), 1632 (υ(C=N), w), 1589 (υ(C=N), s), 1577 (w), 1546 (w), 1471 (m), 1456 (s), 1423 (s), 1399 (w), 1369 (m), 1320 (w), 1291 (w), 1259 (s), 1219 (s), 1189 (w), 1160 (w), 1122 (w), 1100 (w), 1081 (w), 1030 (m), 1000 (w), 977 (w), 942 (w), 883 (w), 850 (m), 811 (m), 769 (s), 760 (s), 747 (w). ^{19}F NMR (470 MHz, CDCl$_3$): δ –145.14. Anal. Calcd, for C$_{54}$H$_{48}$Cl$_2$CoN$_3$F (887.83): C, 73.05; H, 5.45; N, 4.73. Found: C, 72.67; H, 5.23; N, 4.73.

4.5.5. Ar = 2,6-Et$_2$-4-MeC$_6$H$_2$ (**Co5**)

Using the same procedure and molar ratios as described for **Co1**, **Co5** was isolated as a green powder (0.14 g, 56%). FT-IR (KBr cm^{-1}): 3061 (w), 2961 (w), 2928 (w), 2893 (w), 2830 (w), 1626 (υ(C=N), m), 1588 (m),1572 (w), 1515 (w), 1494 (m), 1458 (m), 1448 (w), 1422 (s), 1371 (s), 1340 (w), 1318 (w), 1261 (s), 1189 (w), 1158 (w), 1120 (w), 1098 (w), 1058 (w), 1030 (m), 984 (w), 946 (w), 921 (w), 881 (w), 861 (w), 841 (w), 815 (m), 769 (s), 758 (s), 745 (w). ^{19}F NMR (470 MHz, CDCl$_3$): δ −137.97. Anal. Calcd. for C$_{57}$H$_{55}$Cl$_2$CoN$_3$ (911.91): C, 73.44; H, 5.72; N, 4.59. Found: C, 73.19; H, 5.85; N, 4.50.

4.6. Synthesis of [2,6-{(2,4-(C$_{15}$H$_{13}$)$_2$-6-FC$_6$H$_2$)N=CMe}$_2$C$_5$H$_3$N]CoCl$_2$ (*Co6*)

Using the same procedure as described for **L1**, but using **L6** (0.15 g, 0.135 mmol) and CoCl$_2$ (0.0175 g, 0.135 mmol), **Co6** was isolated as a pale green powder (0.11 g, 73%). FT-IR (KBr cm^{-1}): 3059 (w), 2956 (w), 2930 (w), 2891 (w), 2833 (w), 1618 (υ(C=N), m), 1581 (m), 1570 (w), 1520 (w), 1488 (m), 1454 (w), 1440 (w), 1418 (s), 1374 (m), 1338 (w), 1316 (w), 1264 (s), 1187 (w), 1160 (w), 1124 (w), 1092 (w), 1061 (w), 1028 (m), 980 (w), 941 (w), 918 (w), 887 (w), 852 (w), 833 (m), 812 (w), 766 (s), 754 (s), 720 (w). ^{19}F NMR (470 MHz, CDCl$_3$): δ

-145.83, -146.89. Anal. Calcd. for $C_{81}H_{65}Cl_2CoN_3F_2 \cdot 0.5EtOH$ (1271.30): C, 77.47; H, 5.39; N, 3.31. Found: C, 77.09; H, 5.58; N, 3.48.

4.7. Procedures for the Ethylene Polymerization Runs at 1, 5, and 10 atm

4.7.1. Ethylene Polymerization at 5 and 10 atm Pressure

These runs were performed in a stainless-steel autoclave (250 mL) equipped with a mechanical stirrer and an ethylene pressure and temperature control system. In a typical procedure, the autoclave was evacuated and refilled with nitrogen gas; this process was repeated three times. After the final evacuation, ethylene was introduced to provide an ethylenic atmosphere inside the autoclave, at which point a solution of the corresponding precatalyst (1.5 µmol) in toluene (25 mL) was injected, followed by more toluene (25 mL). Then, the required amount of a co-catalyst (MAO, or MMAO) was loaded, followed by the addition of more toluene (50 mL). Finally, the autoclave was pressurized with ethylene (5 or 10 atm) and stirring commenced at a rate of 400 rpm. Upon completion of the reaction, the stirring was stopped, the reactor was cooled to room temperature, and the pressure slowly released. The contents of the autoclave were quenched with hydrochloric acid (10%) in ethanol and the polymer further washed with ethanol. Finally, the polymer was filtered, dried under reduced pressure at 40 °C, and weighed.

4.7.2. Ethylene Polymerization at 1 atm Pressure

The polymerizations undertaken at 1 atm of C_2H_4 were carried out in a Schlenk vessel. Under an atmosphere of ethylene (ca. 1 atm), the cobalt precatalyst (1.5 µmol) was added to the vessel, followed by toluene (30 mL) and then the required amount of co-catalyst was introduced by syringe. The resulting solution was stirred at 30 °C under an ethylene atmosphere (1 atm). After 30 min, the pressure was slowly released and the solution was quenched with 10% hydrochloric acid in ethanol. The polymer was washed with ethanol, dried under reduced pressure at 40 °C, and then weighed.

5. Conclusions

Five types of unsymmetrical 2,6-bis(arylimino)pyridine cobalt(II) complex (**Co1**–**Co5**), each incorporating one *N*-2,4-bis(dibenzosuberyl)-6-fluorophenyl group together with one sterically and electronically variable *N*-aryl group were successfully prepared. The symmetrical comparator **Co6,** containing two *N*-2,4-bis(dibenzosuberyl)-6-fluorophenyl groups, was also prepared. All compounds, including the free ligands (**L1**–**L6**), were characterized by various spectroscopic techniques, including single crystal X-ray diffraction for **Co1** and **Co2**. Upon activation with MAO or MMAO, **Co1**–**Co6** displayed high activities for ethylene polymerization, with levels reaching as high as 1.15×10^7 g PE mol^{-1} (Co) h^{-1} at 70 °C. Notably, this peak level of performance was observed using the least sterically protected precatalyst, **Co1,** in combination with MAO. Conversely, the most sterically hindered precatalysts, **Co3** and **Co6**, were capable of generating the highest molecular weight polyethylenes in the range of 30.26–33.90 kg mol^{-1} (**Co3**) and 42.90–43.92 kg mol^{-1} (**Co6**). As a key point, the catalytic activity remained significant at temperatures in excess of 70 °C [9.81×10^6 g PE mol^{-1} (Co) h^{-1} at 80 °C and 6.56×10^6 g PE mol^{-1} (Co) h^{-1} at 90 °C]. Evidently, the introduction of a *N*-2,4-bis(dibenzosuberyl)-6-fluorophenyl group contributes to the catalyst's good thermal stability, highlighting a structural feature that could be integrated into industrially relevant catalysts for ethylene polymerization.

Supplementary Materials: The following supporting information can be downloaded at: https://www.mdpi.com/article/10.3390/catal12121569/s1, X-ray diffraction analysis; Table S1: Details of the crystal data and structure refinement parameters for **Co1** and **Co2**. References [72,73] are cited in the Supplementary Materials; Figure S1: ^{19}F NMR spectra of **L1**–**L6**; Figure S2: ^{19}F NMR spectra of **L2**, **L3** and **L6** along with those for **Co2**, **Co3** and **Co6**; Figure S3: GPC curves showing log M_w for the polyethylene produced using **Co1**/MAO as a function of Al:Co molar ratio (runs 5, 8–12, Table 2); Figure S4: GPC curves showing log M_w for the polyethylene produced using **Co1**/MAO as a function of reaction time (runs 5, 13–16, Table 2); Figure S5: GPC curves showing log M_w for the polyethylene

produced using **Co1**/MMAO as a function of Al:Co molar ratio (runs 5, 8–12, Table 3); Figure S6: GPC curves showing log M_w for the polyethylene produced using **Co1**/MMAO as a function of reaction time runs 10, 13–16, Table 3); Figure S7: ^{1}H NMR spectrum of the polyethylene produced using **Co1**/MMAO (run 10, Table 3); recorded in $C_2D_2Cl_4$ at 100 °C; Figure S8: ^{13}C NMR spectrum of the polyethylene produced using **Co1**/MMAO (run 10, Table 3; recorded in deuterated $C_2D_2Cl_4$ at 100 °C.

Author Contributions: Conceptualization, W.-H.S. and G.A.S.; methodology, M.Z.; software, Y.S.; validation, M.Z., W.-H.S. and Y.M.; formal analysis, M.Z.; investigation, M.Z.; resources, Q.Z.; data curation, D.D.S.; writing—original draft preparation, M.Z.; writing—review and editing, G.A.S.; visualization, W.-H.S.; supervision, W.-H.S.; project administration, W.-H.S. All authors have read and agreed to the published version of the manuscript.

Data Availability Statement: All the samples of the organic compounds, cobalt complexes, and data supporting the study are available from the authors.

Conflicts of Interest: There are no conflict of interest to declare.

References

1. Small, B.L.; Brookhart, M.; Bennett, A.M.A. Highly Active Iron and Cobalt Catalysts for the Polymerization of Ethylene. *J. Am. Chem. Soc.* **1998**, *120*, 4049–4050. [CrossRef]
2. Britovsek, G.J.P.; Gibson, V.C.; Kimberley, B.S.; Maddox, P.J.; McTavish, S.J.; Solan, G.A.; White, A.J.P.; Williams, D.J. Novel olefin polymerization catalysts based on iron and cobalt. *Chem. Commun.* **1998**, *7*, 849–850. [CrossRef]
3. Johnson, L.K.; Killian, C.M.; Brookhart, M. New Pd(II)- and Ni(II)-Based Catalysts for Polymerization of Ethylene and α-Olefins. *J. Am. Chem. Soc.* **1995**, *117*, 6414–6415. [CrossRef]
4. Killian, C.M.; Tempel, D.J.; Johnson, L.K.; Brookhart, M. Living Polymerization of r-Olefins Using NiII-α-Diimine Catalysts. Synthesis of New Block Polymers Based on α-Olefins. *J. Am. Chem. Soc.* **1996**, *118*, 11664–11665. [CrossRef]
5. Wang, Z.; Liu, Q.; Solan, G.A.; Sun, W.-H. Recent advances in Ni-mediated ethylene chain growth: N_{imine}-donor ligand effects on catalytic activity, thermal stability and oligo-/polymer structure. *Coord. Chem. Rev.* **2017**, *350*, 68–83. [CrossRef]
6. Edgecombe, B.D.; Stein, J.A.; Frechet, J.M.J. The Role of Polymer Architecture in Strengthening Polymer-Polymer Interfaces: A Comparison of Graft, Block, and Random Copolymers Containing Hydrogen-Bonding Moieties. *Macromolecules* **1998**, *31*, 1292–1304. [CrossRef]
7. Harth, E.M.; Hecht, S.; Helms, B.; Malmstrom, E.E.; Frechet, J.M.J.; Hawker, C.J. The Effect of Macromolecular Architecture in Nanomaterials: A Comparison of Site Isolation in Porphyrin Core Dendrimers and Their Isomeric Linear Analogues. *J. Am. Chem. Soc.* **2002**, *124*, 3926–3938. [CrossRef]
8. Gibson, V.C.; Solan, G.A. Iron-Based and Cobalt-Based Olefin Polymerisation Catalysts. *Top. Organomet. Chem.* **2009**, *2*, 107–158.
9. Gibson, V.C.; Redshaw, C.; Solan, G.A. Bis(imino)pyridines: Surprisingly reactive ligands and a gateway to new families of catalysts. *Chem. Rev.* **2007**, *107*, 1745–1776. [CrossRef]
10. Gibson, V.C.; Solan, G.A. *Catalysis without Precious Metals*; Bullock, R.M., Ed.; Wiley-VCH: Weinheim, Germany, 2010; pp. 111–141.
11. Zhang, W.; Sun, W.-H.; Redshaw, C. Tailoring iron complexes for ethylene oligomerization and/or polymerization. *Dalton Trans.* **2013**, *42*, 8988–8997. [CrossRef]
12. Ma, J.; Feng, C.; Wang, S.; Zhao, K.-Q.; Sun, W.-H.; Redshaw, C.; Solan, G.A. Bi- and tri-dentate imino-based iron and cobalt pre-catalysts for ethylene oligo-/polymerization. *Inorg. Chem. Front.* **2014**, *1*, 14–34. [CrossRef]
13. Flisak, Z.; Sun, W.-H. Progression of Diiminopyridines: From Single Application to Catalytic Versatility. *ACS Catal.* **2015**, *5*, 4713–4724. [CrossRef]
14. Britovsek, G.J.P.; Gibson, V.C.; Kimberley, B.S.; Mastroianni, S.; Redshaw, C.; Solan, G.A.; White, A.J.P.; Williams, D.J. Bis(imino)pyridyl iron and cobalt complexes: The effect of nitrogen substituents on ethylene oligomerisation and polymerisation. *J. Chem. Soc. Dalton Trans.* **2001**, *6*, 1639–1644. [CrossRef]
15. Yue, E.; Zeng, Y.; Zhang, W.; Sun, Y.; Cao, X.-P.; Sun, W.-H. Highly linear polyethylenes using the 2-(1-(2,4-dibenzhydrylnaphthy limino)ethyl)-6-(1-(arylimino)ethyl)pyridylcobalt chlorides: Synthesis, characterization and ethylene polymerization. *Sci. China Chem.* **2016**, *59*, 1291–1300. [CrossRef]
16. Lu, Z.; Liao, Y.; Fan, W.; Dai, S. Efficient suppression of the chain transfer reaction in ethylene coordination polymerization with dibenzosuberyl substituents. *Polym. Chem.* **2022**, *13*, 4090–4099. [CrossRef]
17. Bariashir, C.; Wang, Z.; Du, S.; Solan, G.A.; Huang, C.; Liang, T.; Sun, W.-H. Cycloheptyl-Fused NNO-Ligands as Electronically Modifiable Supports for M(II) (M = Co, Fe) Chloride Precatalysts; Probing Performance in Ethylene Oligo-/Polymerization. *J. Polym. Sci. Part A Polym. Chem.* **2017**, *55*, 3980–3989. [CrossRef]

18. McTavish, S.; Britovsek, G.J.P.; Smit, T.M.; Gibson, V.C.; White, A.J.P.; Williams, D.J. Iron-based ethylene polymerization catalysts supported by bis(imino)pyridine ligands: Derivatization via deprotonation/alkylation at the ketimine methyl position. *J. Mol. Catal. A Chem.* **2007**, *261*, 293–300. [CrossRef]

19. Smit, T.M.; Tomov, A.K.; Britovsek, G.J.P.; Gibson, V.C.; White, A.J.P.; Williams, D.J. The effect of imine-carbon substituents in bis(imino)pyridine-based ethylene polymerisation catalysts across the transition series. *Catal. Sci. Technol.* **2012**, *2*, 643–655. [CrossRef]

20. Sun, W.H.; Hao, P.; Li, G.; Zhang, S.; Wang, W.Q.; Yi, J.; Asma, M.; Tang, N. Synthesis and characterization of iron and cobalt dichloride bearing 2-quinoxalinyl-6-iminopyridines and their catalytic behavior toward ethylene reactivity. *J. Organomet. Chem.* **2007**, *692*, 4506–4518. [CrossRef]

21. Gao, R.; Li, Y.; Wang, F.; Sun, W.-H.; Bochmann, M. 2-Benzoxazolyl-6-[1-(arylimino)ethyl]pyridyliron(II) Chlorides as Ethylene Oligomerization Catalysts. *Eur. J. Inorg. Chem.* **2009**, *2009*, 4149–4156. [CrossRef]

22. Sun, W.-H.; Hao, P.; Zhang, S.; Shi, Q.; Zuo, W.; Tang, X. 2-(Benzimidazolyl)-6-(1-(arylimino)ethyl)pyridyl Complexes as Catalysts for Ethylene Oligomerization and Polymerization. *Organometallics* **2007**, *26*, 2720–2734. [CrossRef]

23. Wang, K.; Wedeking, K.; Zuo, W.; Zhang, D.; Sun, W.-H. Iron(II) and cobalt(II) complexes bearing N-((pyridin-2-yl)methylene)-quinolin-8-amine derivatives: Synthesis and application to ethylene oligomerization. *J. Organomet. Chem.* **2008**, *693*, 1073–1080. [CrossRef]

24. Wang, Z.; Solan, G.A.; Zhang, W.; Sun, W.-H. Carbocyclic-fused *NNN*-pincer ligands as ring-strain adjustable supports for iron and cobalt catalysts in ethylene oligo-/polymerization. *Coord. Chem. Rev.* **2018**, *363*, 92–108. [CrossRef]

25. Pelletier, J.D.A.; Champouret, Y.D.M.; Cadarso, J.; Clowes, L.; Gañete, M.; Singh, K.; Thanarajasingham, V.; Solan, G.A. Electronically variable imino-phenanthrolinyl-cobalt complexes; synthesis, structures and ethylene oligomerisation studies. *J. Organomet. Chem.* **2006**, *691*, 4114–4123. [CrossRef]

26. Jie, S.; Zhang, S.; Wedeking, K.; Zhang, W.; Ma, H.; Lu, X.; Deng, Y.; Sun, W.-H. Cobalt(II) complexes bearing 2-imino-1,10-phenanthroline ligands: Synthesis, characterization and ethylene oligomerization. *C. R. Chim.* **2006**, *9*, 1500–1509. [CrossRef]

27. Jie, S.; Zhang, S.; Sun, W.H.; Kuang, X.; Liu, T.; Guo, J. Iron(II) complexes ligated by 2-imino-1,10-phenanthrolines: Preparation and catalytic behavior toward ethylene oligomerization. *J. Mol. Catal. A Chem.* **2007**, *269*, 85–96. [CrossRef]

28. Han, M.; Oleynik, I.I.; Liu, M.; Ma, Y.; Oleynik, I.V.; Solan, G.A.; Liang, T.; Sun, W.-H. Ring size enlargement in an ortho-cycloalkyl-substituted bis(imino)pyridine-cobalt ethylene polymerization catalyst and its impact on performance and polymer properties. *Appl. Organomet. Chem.* **2021**, *36*, e6529. [CrossRef]

29. Han, M.; Oleynik, I.I.; Ma, Y.; Oleynik, I.V.; Solan, G.A.; Hao, X.; Sun, W.-H. Modulating Thermostability and Productivity of Benzhydryl-Substituted Bis(imino)pyridine-Iron C_2H_4 Polymerization Catalysts through *ortho*-C_nH_{2n-1} 1 (n = 5, 6, 8, 12) Ring Size Adjustment. *Eur. J. Inorg. Chem.* **2022**, *2022*, e202200224. [CrossRef]

30. Xiao, L.; Gao, R.; Zhang, M.; Li, Y.; Cao, X.; Sun, W.-H. 2-(1H-2-Benzimidazolyl)-6-(1-(arylimino)ethyl)pyridyl Iron(II) and Cobalt(II) Dichlorides: Syntheses, Characterizations, and Catalytic Behaviors toward Ethylene Reactivity. *Organometallics* **2009**, *28*, 2225–2233. [CrossRef]

31. Appukuttan, V.K.; Liu, Y.; Son, B.C.; Ha, C.-S.; Suh, H.; Kim, I. Iron and Cobalt Complexes of 2,3,7,8-Tetrahydroacridine-4,5(1H,6H)-diimine Sterically Modulated by Substituted Aryl Rings for the Selective Oligomerization to Polymerization of Ethylene. *Organometallics* **2011**, *30*, 2285–2294. [CrossRef]

32. Zhang, W.; Chai, W.; Sun, W.-H.; Hu, X.; Redshaw, C.; Hao, X. 2-(1-(Arylimino)ethyl)-8-arylimino-5,6,7-trihydroquinoline Iron(II) Chloride Complexes: Synthesis, Characterization, and Ethylene Polymerization Behavior. *Organometallics* **2012**, *31*, 5039–5048. [CrossRef]

33. Sun, W.-H.; Kong, S.; Chai, W.; Shiono, T.; Redshaw, C.; Hu, X.; Guo, C.; Hao, X. 2-(1-(Arylimino)ethyl)-8-arylimino-5,6,7-trihydroquinolylcobalt dichloride: Synthesis and polyethylene wax formation. *Appl. Catal. A* **2012**, *447*, 67–73. [CrossRef]

34. Huang, F.; Xing, Q.; Liang, T.; Flisak, Z.; Ye, B.; Hu, X.; Yang, W.; Sun, W.H. 2-(1-Aryliminoethyl)-9-arylimino-5,6,7,8 tetrahydrocycloheptapyridyl iron(II) dichloride: Synthesis, characterization, and the highly active and tunable active species in ethylene polymerization. *Dalton Trans.* **2014**, *43*, 16818–16829. [CrossRef]

35. Huang, F.; Zhang, W.; Yue, E.; Liang, T.; Hu, X.; Sun, W.-H. Controlling the molecular weights of polyethylene waxes using the highly active precatalysts of 2-(1-aryliminoethyl)-9-arylimino-5,6,7,8tetrahydrocycloheptapyridylcobalt chlorides: Synthesis, characterization, and catalytic behaviour. *Dalton Trans.* **2016**, *45*, 657–666. [CrossRef]

36. Wang, S.; Li, B.; Liang, T.; Redshaw, C.; Li, Y.; Sun, W.-H. Synthesis, characterization and catalytic behavior toward ethylene of 2-[1-(4,6-dimethyl-2-benzhydrylphenylimino)ethyl]-6-[1-(arylimino)ethyl]-pyridylmetal (iron or cobalt) chlorides. *Dalton Trans.* **2013**, *42*, 9188–9197. [CrossRef]

37. Yu, J.; Huang, W.; Wang, L.; Redshaw, C.; Sun, W.H. 2-[1-(2,6-Dibenzhydryl-4-methylphenylimino)ethyl]-6-[1-(arylimino) ethyl]pyridylcobalt(II) dichlorides: Synthesis, characterization and ethylene polymerization behaviour. *Dalton Trans.* **2011**, *40*, 10209–10214. [CrossRef]

38. Yu, J.; Liu, H.; Zhang, W.; Hao, X.; Sun, W.H. Access to highly active and thermally stable iron precatalysts using bulky 2-[1-(2,6-dibenzhydryl-4-methylphenylimino)ethyl]-6-[1-(arylimino)ethyl]pyridine ligands. *Chem. Commun.* **2011**, *47*, 3257–3259. [CrossRef]

39. He, F.; Zhao, W.; Cao, X.-P.; Liang, T.; Redshaw, C.; Sun, W.-H. 2-[1-(2,6-dibenzhydryl-4-chlorophenylimino)ethyl]-6-[1-aryliminoethyl]pyridyl cobalt dichlorides: Synthesis, characterization and ethylene polymerization behaviou. *J. Organomet. Chem.* **2012**, *713*, 209–216. [CrossRef]

40. Cao, X.; He, F.; Zhao, W.; Cai, Z.; Hao, X.; Shiono, T.; Redshaw, C.; Sun, W.-H. 2-[1-(2,6-Dibenzhydryl-4-chlorophenylimino)ethyl]-6-[1-(arylimino)ethyl]pyridyliron(II) dichlorides: Synthesis, characterization and ethylene polymerization behaviour. *Polymer* **2012**, *53*, 1870–1880. [CrossRef]

41. Sun, W.-H.; Zhao, W.; Yu, J.; Zhang, W.; Hao, X.; Redshaw, C. Enhancing the Activity and Thermal Stability of Iron Precatalysts Using 2-(1-{2,6-bis[bis(4fluorophenyl)methyl]-4-methylphenylimino}ethyl)-6-[1-(arylimino)ethyl]pyridines. *Macromol. Chem. Phys.* **2012**, *213*, 1266–1273. [CrossRef]

42. Zhao, W.; Yue, E.; Wang, X.; Yang, W.; Chen, Y.; Hao, X.; Cao, X.; Sun, W.H. Activity and Stability Spontaneously Enhanced Toward Ethylene Polymerization by Employing 2-(1-(2,4-Dibenzhydrylnaphthylimino)Ethyl)-6-(1-(Arylimino)Ethyl)Pyridyliron(II) Dichlorides. *J. Polym. Sci. Part A Polym. Chem.* **2017**, *55*, 988–996. [CrossRef]

43. Wang, S.; Zhao, W.; Hao, X.; Li, B.; Redshaw, C.; Li, Y.; Sun, W.-H. 2-(1-{2,6-Bis[bis(4-fluorophenyl)methyl]-4-methylphenylimino}ethyl)-6-[1(arylimino)ethyl]pyridylcobalt dichlorides: Synthesis, characterization and ethylene polymerization behaviour. *J. Organomet. Chem.* **2013**, *731*, 78–84. [CrossRef]

44. Zhang, W.; Wang, S.; Du, S.; Guo, C.-Y.; Hao, X.; Sun, W.-H. 2-(1-(2,4-Bis((di(4-fluorophenyl)methyl)-6methylphenylimino)ethyl)-6-(1-(arylimino)ethyl)pyridylmetal (iron or cobalt) Complexes: Synthesis, Characterization, and Ethylene Polymerization Behavior. *Macromol. Chem. Phys.* **2014**, *215*, 1797–1809. [CrossRef]

45. Mahmood, Q.; Ma, Y.; Hao, X.; Sun, W.-H. Substantially enhancing the catalytic performance of bis(imino)pyridylcobalt chloride pre-catalysts adorned with benzhydryl and nitro groups for ethylene polymerization. *Appl. Organomet. Chem.* **2019**, *33*, e4857. [CrossRef]

46. Mahmood, Q.; Zeng, Y.; Wang, X.; Sun, Y.; Sun, W.-H. Advancing polyethylene properties by incorporating NO_2 moiety in 1,2-bis(arylimino)acenaphthylnickel precatalysts: Synthesis, characterization and ethylene polymerization. *Dalton Trans.* **2017**, *46*, 6934–6947. [CrossRef]

47. Mitchell, N.E.; Anderson, W.C., Jr.; Long, B.K. Mitigating Chain-Transfer and Enhancing the Thermal Stability of Co-Based Olefin Polymerization Catalysts through Sterically Demanding Ligands. *J. Polym. Sci., Part A Polym. Chem.* **2017**, *55*, 3990–3995. [CrossRef]

48. Lai, J.; Zhao, W.; Yang, W.; Redshaw, C.; Liang, T.; Liu, Y.; Sun, W.-H. 2-[1-(2,4-Dibenzhydryl-6-methylphenylimino)ethyl]-6-[1-(arylimino)ethyl]pyridylcobalt(II) dichlorides: Synthesis, characterization and ethylene polymerization behaviour. *Polym. Chem.* **2012**, *3*, 787–793. [CrossRef]

49. Zhao, W.; Yu, J.; Song, S.; Yang, W.; Liu, H.; Hao, X.; Redshaw, C.; Sun, W.-H. Controlling the ethylene polymerization parameters in iron pre-catalysts of the type 2-[1-(2,4-dibenzhydryl-6-methylphenylimino)ethyl]-6-[1-(arylimino)ethyl]pyridyliron dichloride. *Polymer* **2012**, *53*, 130–137. [CrossRef]

50. Guo, L.; Zada, M.; Zhang, W.; Vignesh, A.; Zhu, D.; Ma, Y.; Liang, T.; Sun, W.-H. Highly linear polyethylenes tailored by 2,6-bis[1-(*p*-dibenzocycloheptylarylimino)ethyl]pyridylcobalt dichlorides. *Dalton Trans.* **2019**, *48*, 5604–5613. [CrossRef]

51. Guo, L.; Zhang, W.; Cao, F.; Jian, Y.; Zhang, R.; Ma, Y.; Solan, G.A.; Sun, W.-H. Remote dibenzocycloheptyl substitution on a bis(arylimino)pyridyl-iron ethylene polymerization catalyst; enhanced thermal stability and unexpected effects on polymer properties. *Polym. Chem.* **2021**, *12*, 4214–4225. [CrossRef]

52. Zada, M.; Guo, L.; Ma, Y.; Zhang, W.; Flisak, Z.; Sun, Y.; Sun, W.-H. Activity and Thermal Stability of Cobalt(II)-Based Olefin Polymerization Catalysts Adorned with Sterically Hindered Dibenzocycloheptyl Groups. *Molecules* **2019**, *24*, 2007. [CrossRef] [PubMed]

53. Zada, M.; Vignesh, A.; Guo, L.; Suo, H.; Ma, Y.; Liu, H.; Sun, W.-H. NNN type iron(II) complexes consisting sterically hindered dibenzocycloheptyl groups: Synthesis and catalytic activity towards ethylene polymerization. *Mol. Catal.* **2020**, *492*, 110981. [CrossRef]

54. Bariashir, C.; Zhang, R.; Vignesh, A.; Ma, Y.; Liang, T.; Sun, W.-H. Enhancing Ethylene Polymerization of *NNN*-Cobalt(II) Precatalysts Adorned with a Fluoro-substituent. *ACS Omega* **2021**, *6*, 4448–4460. [CrossRef] [PubMed]

55. Zheng, Q.; Li, Z.; Han, M.; Xiang, J.; Solan, G.A.; Liang, T.; Sun, W.-H. Fluorinated cobalt catalysts and their use in forming narrowly dispersed polyethylene waxes of high linearity and incorporating vinyl functionality. *Catal. Sci. Technol.* **2021**, *11*, 656–670. [CrossRef]

56. Zheng, Q.; Zuo, Z.; Ma, Y.; Liang, T.; Yang, X.; Sun, W.-H. Fluorinated 2,6-bis(arylimino)pyridyl iron complexes targeting bimodal dispersive polyethylene: Probing chain termination pathways via combined experimental and DFT. *Dalton Trans.* **2022**, *51*, 8290–8302. [CrossRef]

57. Meiries, S.; Speck, K.; Cordes, D.B.; Slawin, A.M.Z.; Nolan, S.P. [Pd(IPr*OMe)(acac)Cl]: Tuning the N-Heterocyclic Carbene in Catalytic C−N Bond Formation. *Organometallics* **2012**, *32*, 330–339. [CrossRef]

58. Zada, M.; Guo, L.; Zhang, R.; Zhang, W.; Ma, Y.; Solan, G.A.; Sun, Y.; Sun, W.-H. Moderately branched ultra-high molecular weight polyethylene by using N,N′-nickel catalysts adorned with sterically hindered dibenzocycloheptyl groups. *Appl. Organomet. Chem.* **2019**, *33*, e4749. [CrossRef]

59. Zada, M.; Vignesh, A.; Guo, L.; Zhang, R.; Zhang, W.; Ma, Y.; Sun, Y.; Sun, W.-H. Sterically and Electronically Modified Aryliminopyridyl-Nickel Bromide Precatalysts for an Access of Branched Polyethylene with Vinyl/Vinylene End Groups. *ACS Omega* **2020**, *5*, 10610–10625. [CrossRef]

60. Britovsek, G.J.P.; Bruce, M.; Gibson, V.C.; Kimberley, B.S.; Maddox, P.J.; Mastroianni, S.; McTavish, S.J.; Redshaw, C.; Solan, G.A.; Stromberg, S.; et al. Iron and Cobalt Ethylene Polymerization Catalysts Bearing 2,6-Bis(Imino)Pyridyl Ligands: Synthesis, Structures, and Polymerization Studies. *J. Am. Chem. Soc.* **1999**, *121*, 8728–8740. [CrossRef]

61. Britovsek, G.J.P.; Gibson, V.C.; Spitzmesser, S.K.; Tellmann, K.P.; White, A.J.P.; Williams, D.J. Cationic 2,6-bis(imino)pyridine iron and cobalt complexes: Synthesis, structures, ethylene polymerisation and ethylene/polar monomer co-polymerisation studies. *J. Chem. Soc. Dalton Trans.* **2002**, *6*, 1159–1171. [CrossRef]

62. Cantalupo, S.A.; Ferreira, H.E.; Bataineh, E.; King, A.J.; Petersen, M.V.; Wojtasiewicz, T.; DiPasquale, A.G.; Rheingold, A.L.; Doerrer, L.H. Synthesis with Structural and Electronic Characterization of Homoleptic Fe(II)- and Fe(III)-Fluorinated Phenolate Complexes. *Inorg. Chem.* **2011**, *50*, 6584–6596. [CrossRef] [PubMed]

63. Yuan, J.; Shi, W.-B.; Kou, H.-Z. Syntheses, crystal structures and magnetism of azide-bridged five-coordinate binuclear nickel(II) and cobalt(II) complexes. *Transit. Met. Chem.* **2015**, *40*, 807–811. [CrossRef]

64. Britovsek, G.J.P.; Gibson, V.C.; Hoarau, O.D.; Spitzmesser, S.K.; White, A.J.P.; Williams, D.J. Iron and Cobalt Ethylene Polymerization Catalysts: Variations on the Central Donor. *Inorg. Chem.* **2003**, *42*, 3454–3465. [CrossRef] [PubMed]

65. Tomov, A.K.; Gibson, V.C.; Britovsek, G.J.P.; Long, R.J.; Meurs, M.V.; Jones, D.J.; Tellmann, K.P.; Chirinos, J.J. Distinguishing Chain Growth Mechanisms in Metal-catalyzed Olefin Oligomerization and Polymerization Systems: C_2H_4/C_2D_4 Co-oligomerization/Polymerization Experiments Using Chromium, Iron, and Cobalt Catalysts. *Organometallics* **2009**, *28*, 7033–7040. [CrossRef]

66. Barbaro, P.; Bianchini, C.; Giambastiani, G.; Rios, I.G.; Meli, A.; Oberhauser, W.; Segarra, A.M.; Sorace, L.; Toti, A. Synthesis of New Polydentate Nitrogen Ligands and Their Use in Ethylene Polymerization in Conjunction with Iron(II) and Cobalt(II) Bis-halides and Methylaluminoxane. *Organometallics* **2007**, *26*, 4639–4651. [CrossRef]

67. Liu, M.; Jiang, S.; Ma, Y.; Solan, G.A.; Sun, Y.; Sun, W.-H. CF_3O-Functionalized Bis(arylimino)pyridine−Cobalt Ethylene Polymerization Catalysts: Harnessing Solvent Effects on Performance and Polymer Properties. *Organometallics* **2022**, *41*, 3237–3248. [CrossRef]

68. Pooter, M.D.; Smith, P.B.; Dohrer, K.K.; Bennett, K.F.; Meadows, M.D.; Smith, C.G.; Schouwenaars, H.P.; Geerards, R.A. Determination of the Composition of Common linear low Density Polyethylene Copolymers by ^{13}C-NMR Spectroscopy. *J. Polym. Sci.* **1991**, *42*, 399–408. [CrossRef]

69. Galland, G.B.; Quijada, R.; Rojas, R.; Bazan, G.; Komon, Z.J.A. NMR Study of Branched Polyethylenes Obtained with Combined Fe and Zr Catalysts. *Macromolecules* **2002**, *35*, 339–345. [CrossRef]

70. Hansen, E.W.; Blom, R.B.; Bade, O.M. N.m.r. characterization of polyethylene with emphasis on internal consistency of peak intensities and estimation of uncertainties in derived branch distribution numbers. *Polymer* **1997**, *38*, 4295–4304. [CrossRef]

71. Semikolenova, N.V.; Sun, W.-H.; Soshnikov, I.E.; Matsko, M.A.; Kolesova, O.V.; Zakharov, V.A.; Bryliakov, K.P. Origin of "Multisite-like" Ethylene Polymerization Behavior of the Single-Site Nonsymmetrical Bis(imino)pyridine Iron(II) Complex in the Presence of Modified Methylaluminoxane. *ACS Catal.* **2017**, *7*, 2868–2877. [CrossRef]

72. Sheldrick, G.M. Crystal structure refinement with SHELXL. *Acta Crystallogr. C Struct. Chem.* **2015**, *71*, 3–8. [CrossRef] [PubMed]

73. Sheldrick, G.M. SHELXT—Integrated space-group and crystal structure determination. *Acta Crystallogr. A Found. Adv.* **2015**, *71*, 3–8. [CrossRef] [PubMed]